HAL
open science

Effect of hydrogen addition on NOx formation in high-pressure counter-flow premixed CH4/air flames

Stéphanie de Persis, Mahmoud Idir, Julien Molet, Laure Pillier

To cite this version:

Stéphanie de Persis, Mahmoud Idir, Julien Molet, Laure Pillier. Effect of hydrogen addition on NOx formation in high-pressure counter-flow premixed CH4/air flames. International Journal of Hydrogen Energy, 2019, 44 (41), pp.23484-23502. 10.1016/j.ijhydene.2019.07.002 . hal-02297725

HAL Id: hal-02297725

https://hal.science/hal-02297725v1

Submitted on 13 Nov 2020

HAL is a multi-disciplinary open access archive for the deposit and dissemination of scientific research documents, whether they are published or not. The documents may come from teaching and research institutions in France or abroad, or from public or private research centers.

L'archive ouverte pluridisciplinaire **HAL**, est destinée au dépôt et à la diffusion de documents scientifiques de niveau recherche, publiés ou non, émanant des établissements d'enseignement et de recherche français ou étrangers, des laboratoires publics ou privés.

Effect of hydrogen addition on NOx formation in high-pressure counter-flow premixed CH_4/air flames

Stéphanie de Persis[1,2*], Mahmoud Idir[1], Julien Molet[1] and Laure Pillier[3]

Affiliations

[1]ICARE, Institut de Combustion, Aérothermique, Réactivité, Environnement, UPR3021 CNRS, 1C Av. de la recherche scientifique, 45071 Orléans, France

[2]Univ. Orléans, Château de la source, Avenue du parc floral, 45067 Orléans, France

[3]Univ. Lille, CNRS, UMR8522 - PC2A - PhysicoChimie des Processus de Combustion et de l'Atmosphère, F-59000 Lille, France

[*]Corresponding author: S. de Persis, depersis@cnrs-orleans.fr

Abstract

A laboratory-scale laminar counterflow burner was used to investigate NO formation in high pressure premixed CH_4/H_2/air flames. New experimental results on NO measurements by LIF were obtained at high pressure in CH_4/H_2/air flames with H_2 content fixed at 20% in the fuel at pressures ranging from 0.1 to 0.7 MPa and an equivalence ratio progressively decreased from 0.74 to 0.6. The effects of hydrogen addition, equivalence ratio and pressure are discussed. These results are satisfactorily compared to the simulations using two detailed mechanisms: GDF®kin3.0_NOmecha2.0 and the mechanism from Klippenstein et al., which are the most recent high-pressure NOx formation mechanisms available in the literature. A kinetic analysis based on Rate of Production/Rate of Consumption and sensitivity analyses of NO is then presented to identify the main pathways that lead to the formation and consumption of NO. In addition, the effect of hydrogen addition on NO formation pathways is described and analysed.

Keywords (max 6): Hydrogen, NOx formation, high pressure flames, kinetic analysis

1. Introduction

The addition of hydrogen to a hydrocarbon flame is of great interest as it improves the burning stability, the combustion efficiency, and reduces the greenhouse gas and pollutant emissions, such as NO_x, CO_2, CO, unburned hydrocarbons and soot particles [1]. Blending hydrogen in the fuel allows shortening the ignition delay time [2]. As it allows the extension of flammability limits towards fuel-lean conditions [3], where the emission of NO_x is significantly reduced, ultra-lean hydrogen-enriched flames can be obtained. An illustration of the interest of hydrogen-enriched combustion is the performance testing of Hythane® fuel (registered trademark for a blend of 20% hydrogen and 80% natural gas by volume) in "test" public transport [4-6]. Theoretically, the addition of hydrogen to a hydrocarbon fuel may reduce the prompt-NO due to the decrease in hydrocarbon radicals in the flame, assuming a constant temperature. However, the addition of hydrogen may cause a rise in the flame temperature [7], which would result in an increase in thermal-NO formation. In addition, the NO from the NNH mechanism [3] may increase compared to pure hydrocarbon flames. The combined effects of these factors determine the net influence of hydrogen addition on NO_x emission in hydrocarbon flames.

Gauducheau et al. [8] performed a numerical study, using GRImech2.11 [9], of the effect of including a small amount of hydrogen (20% in fuel) in lean methane-air flames at high pressure (3 MPa). They concluded that the major effect of hydrogen blending is the improved behaviour of the flame in response to strain, which indicates that the flame is able to withstand higher turbulence levels when hydrogen is included.

Rortveit et al. [10] reported a comparison of low-NO_x burners for combustion of methane and hydrogen mixtures. The effect of hydrogen addition to natural gas or methane on NOx emissions were found to be significantly dependent on burner type.

In 2004, Hawkes and Chen [11] reported a direct numerical simulation (DNS) of hydrogen-enriched (29% of H_2 in fuel) lean (ϕ=0.52) premixed methane–air flames in order to study the possible effects of H_2 enrichment on flame stability and pollutant formation. The authors observed a higher turbulent flame speed for the enriched flame, which is consistent with enhanced blow-off stability observed in experiments. A 50% increase in NO production per unit heat release was also observed for the enriched flame relative to the pure methane flame, attributed to locally high temperatures and radical levels.

Naha and Aggarwal [12] investigated numerically the effect of hydrogen addition on NO emissions in non-premixed methane flames and showed that the observed decrease in the prompt-NO due to hydrogen addition is balanced by the corresponding increase in the thermal-NO, and the total NO is essentially unaffected by hydrogen addition.

Guo et al. [3] investigated, by numerical simulation using the GRIMech3.0 mechanism [13], the effect of hydrogen addition on flammability limit and NOx emissions in ultra-lean (ϕ=0.4 – 0.7) counterflow CH_4/air premixed flames at atmospheric pressure. The authors showed that addition of hydrogen (0 to 60% in fuel) increases NO emission in their flames if the equivalence ratio is kept constant. They concluded that this rise in NO formation rate is mainly caused by the rise of the NNH intermediate route, except for the flames with a very low equivalence ratio and at lower hydrogen fraction where the increase in the N_2O intermediate route is more significant.

Coppens at al. [14, 15] measured NO_x concentrations in CH_4-H_2-O_2-N_2 atmospheric pressure laminar flat flames with varying H_2 content (from 0 to 35%), equivalence ratio (0.7-1.4) and dilution ratio (O_2 in oxidizer from 0.16 to 0.209). The authors observed that in lean flames, enrichment by hydrogen has little effect on NO emissions, while in rich flames the concentration of NO decreases significantly due to a reduction of the prompt-NO formation.

De Ferrieres et al. [16] investigated, experimentally and numerically (with GDFkin®3.0 mechanism) the effect of hydrogen addition on the flame structure of a natural gas low pressure (8 kPa) premixed flame (stable species measurements with quartz probe sampling and GC/FTIR analyses). Their main conclusions were: i) the C_1 hydrocarbons oxidation sequence initiated by H-abstraction by H, OH and O from methane is favoured when H_2 is added; ii) the C_2 hydrocarbons sequence is consequently disfavoured, which reduces the mole fraction of acetylene, considered as the main PAH and soot precursor. This was also observed by Biet et al. [17].

Parente et al. [18] studied MILD (Moderate or Intense Low-oxygen Dilution) combustion in an industrial burner fed with hydrogen enriched fuels. They developed a simple NO formation mechanism, based on the thermal and prompt routes. They found a relatively good agreement between their Eddy Dissipation Concept (EDC) model and experimental measurements. MILD combustion was found to be a solution to reduce the NO concentration in the diffusion flames. They also demonstrated in [19] that the NNH and N_2O routes were the dominant sources for the overall NO production when hydrogen-enriched fuels were involved. Mardani and Tabejamaat [20] investigated the NOx formation in a turbulent H_2/CH_4 flame under MILD conditions. They also confirmed that the NNH and N_2O routes were the most important pathways. Gao et al. [21] studied NOx formation in hydrogen-methane turbulent diffusion flame under MILD conditions. Three flames with the oxygen mass fraction varying from 3% to 9% and hydrogen content in fuel from 11 to 30% were studied and compared with experiments. Analysis of the NO formation mechanisms shows that the NNH and prompt routes are enhanced by hydrogen addition, while the influence on N_2O formation and thermal route remains limited.

Hu et al. [22] reported a numerical study (GRIMech30 in PREMIX) on laminar burning velocity and NO formation of premixed methane–hydrogen–air flames at atmospheric pressure. Hydrogen fractions in the fuel were varied from 0% to 100% with interval of 10%. Three flames with different equivalence ratios were studied: lean (ϕ=0.8), stoichiometric (ϕ=1) and rich (ϕ=1.2). The unstretched laminar burning velocity, adiabatic flame temperature, and mole fractions of H, OH and NO were obtained at various equivalence ratios and hydrogen fractions. They observed an increase of laminar burning velocity as well as the adiabatic flame temperature with the increase of hydrogen fraction. They reported that in the stoichiometric flame, hydrogen addition has little effect on NO due to the Zeldovich thermal-NO mechanism, while in the fuel-rich flames, NO concentration decreased significantly due to the Fenimore prompt-NO mechanism. This decrease was attributed to the reduced availability of hydrocarbon radicals, which are major precursors of the Fenimore prompt-NO mechanism.

Wang et al. [23] numerically studied the effect of hydrogen addition on methane–air mixtures combustion. The stoichiometric methane–hydrogen–air freely propagating laminar premixed flames at normal temperature and pressure were calculated by using the PREMIX code with the GRImech3.0 mechanism [13], at equivalence ratio from 0.85 to 1. The hydrogen volumetric fraction in the methane–hydrogen fuel blends is 0-40%. The authors showed that the promotion of the chemical reactions with hydrogen addition is due to the increase of H, O and OH mole fractions in the flame as hydrogen is added. They also concluded that aldehydes emissions of methane combustion are reduced when hydrogen is added whereas there is only a slight effect on NO formation.

Sepman et al. [24] performed NO measurements by Laser Induced Fluorescence in rich premixed CH_4/H_2/air, C_2H_6/H_2/air and C_3H_8/H_2/air premixed flat flames at atmospheric pressure. They found a modest reduction of NO mole fraction with hydrogen addition. This decrease in NO is more distinct in methane and propane flames, and more modest for ethane.

Computations indicate that the decrease in prompt-NO formation with hydrogen addition arises from the concomitant decrease in CH mole fraction.

Zahedi and Yousefi [25] studied numerically the effect of pressure and hydrogen addition on NO formation in a methane-air stoichiometric flame, using the GRImech3.0 mechanism [13]. They showed a slight increase of NO concentration when H_2 is added (10 and 20 % in the mixture) at atmospheric pressure and a strong increase when pressure increases from 0.1 to 0.5 MPa.

More recently, Ying and Liu [26] investigated the chemical effects of hydrogen on methane flames. Stoichiometric methane-air flames were conducted at atmospheric pressure and H_2 was varied from 0 to 20%. The effect of H_2 addition was numerically studied by the fictive species method. A special attention was paid on the formation of soot precursor and oxygenated air pollutants. The authors confirmed that NOx emission concentration decreases as hydrogen is added into the fuel because of the more dominant dilution and thermal effects on suppressing NO formation, even if the chemical effects of hydrogen addition actually promote the production of NO.

Very recently, Wei et al. [27, 28] studied the effects of H_2 and CO_2 addition on the heat transfer characteristics and the emission characteristics of laminar premixed biogas–hydrogen impinging flames (for constant equivalence ratio kept to 1.2; H_2 volume fraction varied from 10 to 50% and CO_2 volume fraction ranging from 25 to 50%). Their numerical (PREMIX with GRIMech3.0) and experimental studies showed that thermal, NNH and N_2O routes increase with the increase of H and the increase of temperature. They attributed the decrease of prompt-NO to the improved premixed combustion that implies lower available hydrocarbon radicals for the initiation reaction. Moreover, they concluded that the contribution of the NNH route is reduced while that of prompt-NO rises when the equivalence ratio is increased. The

contributions of N_2O and thermal routes were found to be maximum in stoichiometric conditions.

Riahi et al. [29] investigated experimentally a non-premixed CH_4 - H_2/ Air - O_2 turbulent flame in lean regime in a coaxial burner. The influence of equivalence ratio on the flame characteristics was studied and higher emissions of NOx were observed in lean flames.

Acero et al. [30] presented a numerical study (with GRImech2.11 [9]) of the effect of hydrogen addition (5-15%) on NO formation in a biogas stoichiometric flame. Only a slight increase of NO concentration is observed in their conditions.

The previous literature review shows that, as far as we know, no experimental measurements of NO profiles in high pressure counterflow premixed CH_4/H_2/air flames are available in the literature. It also shows that methane/hydrogen flames modelling is usually performed using the GRImech3.0 mechanism [13] (or GRImech2.11 [9]) in which the prompt-NO pathway is initiated by the Fenimore reaction: $CH+N_2=HCN+N$. However, particular attention has been paid recently to the prompt-NO formation pathway in flames and it has been demonstrated that the reaction $CH + N_2 = HCN + N$ (known to be spin forbidden) has to be replaced by the reaction $CH + N_2 = NCN + H$ [31, 32].

Very recently, Lamoureux et al. [33] proposed a final version of their new detailed NOx chemistry sub-mechanism, named NOmecha2.0, validated at high temperature on a large experimental database obtained in laminar premixed flames, jet-stirred and plug-flow reactors under sub-atmospheric and atmospheric pressure conditions. This mechanism (GDFkin®3.0_NOmecha2.0: NOmecha2.0 [33] associated to GDFkin®3.0 [34]) was very recently validated in our high pressure counterflow CH_4/air flames [35] and compared to the mechanism from Klippenstein et al. [36], which is the most recent high pressure NOx formation mechanism available in the literature. In the present work, GDFkin®3.0_NOmecha2.0 [35] and Klippenstein [36] mechanisms will be used for validation in high pressure CH_4/H_2/air flames.

In this work, we present new experimental and numerical results: NO mole fraction profiles were measured by Laser Induced Fluorescence in laminar high pressure (up to 0.7 MPa) counterflow lean CH_4/H_2/air flames. H_2 content was fixed to 20% in the fuel; i.e. $XH_2/(XH_2+XCH_4) = 0.2$ (with X the mole fraction) and the equivalence ratio was progressively decreased from 0.74 to 0.6. The experimental NO profiles were then compared with modelling using the LOGEsoft software (LOGEresearch v1.10.0 [37]) and the two mechanisms: GDFkin®3.0_NOmecha2.0 [35] and Klippenstein [36] mechanisms.

To better understand the effect of hydrogen addition and the effect of reducing the equivalence ratio on NO formation, a kinetic analysis was performed based on rate of production and consumption computations. The relative contribution of each NO formation pathways (thermal, prompt, N_2O and NNH) is discussed. To identify elementary reactions that dominate the formation/consumption of NO, sensitivity analyses were also conducted.

2. Experimental

The experimental facility used in this work, including the high pressure burner and the Laser Induced Fluorescence system, has been detailed previously in [38-40], an overview is presented here.

2.1. High pressure burner and flames conditions

The high pressure burner consists of two twin counterflow converging burners placed in a high pressure vessel, equipped with optical accesses. Each burner is composed of two co-annular nozzles of 7 mm and 13 mm diameters, which were aerodynamically shaped to obtain a uniform velocity profile at their exit. The distance between the burners is fixed at 10 mm. A nitrogen co-flow isolates the flame from the surrounding gases. The burners are cooled by water circulation at a fixed temperature between 30 and 50°C depending on the flame conditions, to

avoid water condensation on their surfaces. The pressure within the vessel is controlled with a pressure transducer and a control valve. Gas flows are monitored by Brooks mass flowmeters through a Labview program.

Laminar lean premixed CH_4/H_2/air flames were studied in this work, with 20% of H_2 substituted to CH_4 (ie, $XH_2/(XH_2+XCH_4)$ =0.2, with X the mole fraction). In this case, two expressions of the equivalence ratio can be defined:

- the overall equivalence ratio: $$\phi_{CH} = 2*\left(\frac{XCH_4}{XO_2}\right)+\frac{1}{2}*\left(\frac{XH_2}{XO_2}\right) \quad (1)$$

- and the equivalence ratio relative to methane: $$\phi_C = 2*\left(\frac{XCH_4}{XO_2}\right) \quad (2)$$

In order to investigate the influence of hydrogen addition, we compared a CH_4/air flame with and without hydrogen addition with the same C/O ratio; ie. ϕ_C=0.7. This lean methane flame was previously studied in [35, 40]. Hydrogen addition to CH_4/air flames allows to extend the flammability limits towards very lean conditions. In this work, the equivalence ratio of the CH_4/H_2/air flames was progressively decreased from ϕ_C=0.7 to 0.57 or ϕ_{CH}= 0.74 to 0.6. Below those values of equivalence ratios, the flames became unstable. As for our previous work [35, 40], the pressure was varied from 0.1 to 0.7 MPa. Figure 1 shows pictures of the CH_4/H_2/air flames stabilised in this work. As mentioned elsewhere [35, 40], a stabilisation criterion was defined, using a telescopic sight with high magnification (allowing to distinguish a wire of 50 µm), placed on one of the visualisation window of the chamber in order to scrutinise the flamefronts. For each pressure condition, flames were considered as stable if their central shape appear flat in a diameter greater than the nozzle diameter (7 mm), and their position above the burner do not fluctuate by more than +/- 50 µm around their average position.

Flame conditions are summarised in Table 1, together with adiabatic flame temperatures T_f and laminar flame velocities S_L computed for a free flame configuration using LOGEsoft software (LOGEresearch v1.10.0 [37]) with GDFkin®3.0_NOmecha2.0 [35]. Note that the flame with equivalence ratio ϕ_C=0.61 could not be stabilised at 0.7 MPa and the flame with ϕ_C=0.57 was stabilised only at 0.3 MPa.

2.2. Laser Induced Fluorescence measurements

For LIF measurements of NO in the A-X(0,0) vibrational band, the wavelength around 226 nm was obtained by mixing the frequency-doubled output of the dye laser (Quantel TDL+, mixture of Rhodamine 590 and 610) with the residual infrared radiation from the pumping injection seeded Nd-YAG laser (Quantel Brillant B, repetition rate 10 Hz, 6 ns pulses, linewidth 0.06 cm^{-1}). The laser energy was reduced to 100 µJ to perform LIF measurements in the linear regime. The beam was focused at the centre of the burner and the fluorescence signal was collected at right angle through a spectrometer and a photomultiplier. The probed volume was 160 µm in height and 6.4 mm in width.

As demonstrated in our previous work [40], LIF excitation through the $P_1(23,5)$, $Q_1+P_{21}(14,5)$, $Q_2+R_{12}(20,5)$ line (λ= 226.03 nm) in the A-X(0,0) vibrational band and signal collection through the A-X(0,1) band (centred at 236 nm with a 2.8 nm bandpass) was the best compromise to maximise the NO LIF signal and minimise interferences in our flame conditions. The NO LIF signal was analysed with the same procedure as in [40], the spectral overlap function, the fluorescence quantum yield and the Boltzmann fraction were calculated along each flame and variations of those parameters were found negligible at a given pressure. A calibration procedure was then applied for each flame, consisting in doping the flame with known small amounts of NO to perform a calibration plot. The experimental uncertainties reached ± 20% for all flames.

3. Modelling

The main formation paths of NO in flames are: the thermal-NO [41], the prompt-NO [42], the NNH [43] and the N_2O [44] routes. However, recent work on the prompt-NO formation pathway in flames has shown that the reaction CH + N_2 = HCN + N (known to be spin forbidden) has to be replaced by the reaction CH + N_2 = NCN + H [31, 32]. To compare experimental NO mole fraction profiles to the simulated ones, two reaction mechanisms including the updated prompt-NO pathway were used: GDFkin®3.0 associated to NOmecha2.0 [35], named GDFkin®3.0_NOmecha2.0, developed by our group; and the mechanism from Klippenstein et al. [36], named here Klippenstein mechanism. Table 2 compares the NO formation sub-mechanisms (reactions and associated rate constants) included in the two mechanisms (GDFkin®3.0_NOmecha2.0 [35] and Klippenstein [36]). The comparison of the two reaction mechanisms shows that: i) thermal and NNH reaction mechanisms are identical in both mechanisms; ii) the N_2O reaction pathways are identical in both mechanisms (same reactions) but the rate constant values are different and iii) for the prompt-NO pathway and the NCN chemistry, significant differences are observed in terms of reactions and rate constants, particularly for the description of the chemistry of NCN.

Kinetic modelling of atmospheric and high-pressure counterflow CH_4/H_2/air flames was carried out using the LOGEsoft software (LOGEresearch v1.10.0 [37]) with the counterflow flame module. Calculations were performed by solving the energy equation in the case of an adiabatic and isobaric system and thermo-diffusion effects were taken into account. The adaptive mesh parameters GRAD and CURV were fixed to 1.0 and 1.5 respectively in LOGEsoft, with a number of 300 grid points. The solution is grid-independent.

The calculated NO mole fraction profiles with and without considering the radiation heat loss were carried out in our CH_4/air flames [35], showing a weak influence (< 10%) on the

temperature and NO mole fraction profiles, for all the flame conditions. Radiation effects were then neglected in the present CH_4/H_2/air flames.

The kinetic analyses carried out in this paper consisted in reaction pathways (rate-of-consumption ROC/production ROP and net flux analyses) and sensitivity analysis. Rates of production and consumption as a function of the distance from the bottom burner were computed for each species with LOGESoft [37]. Net rates were considered by summing ROC and ROP after integration over the whole flame domain. It is thus possible to have global information on which reaction contributes to the production or consumption of a given species. To identify elementary reactions that dominate the formation/consumption of NO, sensitivity analyses were also conducted (only the 20 most contributive reactions were considered).

4. Results and discussions

4.1. Experimental results

Figure 2 shows the mole fraction profiles of NO in the methane/hydrogen/air flames at equivalence ratio Φ_{CH}= 0.74 (Figure 2a); 0.7 (Figure 2b) and 0.65 (Figure 2c) as a function of pressure. For the flame at Φ_{CH}= 0.74, the NO mole fraction increases from 0.1 to 0.3 MPa and then remains almost constant when pressure increases further to 0.5 and 0.7 MPa (see Figure 2a). At Φ_{CH}= 0.7 and 0.65, the maximum NO mole fractions (XNO_{max}) increases with pressure, except at 0.5 MPa where XNO_{max} values are slightly lower than the values obtained at 0.1 MPa. All the profiles are centered at a distance of 0.5-0.55 cm from the bottom burner. The positions of the two flamefronts differ slightly with pressure, the distance between the two flamefronts tends to increase when pressure increases for the Φ_{CH}= 0.74 and 0.7 flames, while it remains almost constant for Φ_{CH}= 0.65. The variation of XNO_{max} as a function of equivalence ratio shows that at a given pressure, the NO concentration decreases with equivalence ratio, as expected.

4.2. Comparison between experimental and calculated NO mole fraction profiles

As mentioned above, two detailed kinetic mechanisms were used: GDFkin®3.0_NOmecha2.0 [35] and Klippenstein [36] mechanisms. In both cases, the adiabatic assumption was used in the calculation. The temperature profiles predicted by both mechanisms are shown in Figure A in the supplementary file. This figure shows that, whatever the conditions, there is no significant difference in the temperature profiles predicted by the two mechanisms in terms of both shape and maximum temperature.

Figure 3 compares the experimental and calculated NO mole fraction profiles in the CH_4/H_2/air flames for ϕ_{CH}=0.74, ϕ_{CH}=0.7, ϕ_{CH}=0.65 and ϕ_{CH}=0.6 at pressures ranging from 0.1 to 0.7MPa. The NO profiles present a "bell" shape due to NO formation in the burned gases and are all centered at a distance of 0.5-0.55 cm from the bottom burner.

For ϕ_{CH}=0.74 (Figure 3a), both mechanisms reproduce correctly the shapes of the NO profiles for all the pressure conditions. At 0.1 and 0.3 MPa, the experimental profile is slightly shifted to the right, i.e. towards the top burner, compared to the calculated profiles. Both mechanisms are in good agreement with experiments and present closed results. GDFkin®3.0_NOmecha2.0 predicts slightly lower maximum NO mole fraction than Klippenstein at 0.1 and 0.3 MPa, and slightly higher at 0.5 and 0.7 MPa.

For ϕ_{CH}=0.7 (Figure 3b), both mechanisms are in satisfactory agreement with experiments at 0.1 and 0.7 MPa but overestimate the maximum NO mole fraction at 0.3 and 0.5 MPa. The distance between the flamefronts is satisfactorily predicted by both mechanisms at 0.1MPa but overestimated for higher pressures.

For ϕ_{CH}=0.65 (Figure 3c), the two mechanisms predict the NO mole fraction profile well at 0.1 MPa. At 0.3 MPa, the calculated profiles obtained with the two mechanisms underestimate the NO mole fractions and slightly overestimate the distance between the flamefronts. At 0.5 MPa,

both mechanisms overpredict the maximum value of the NO mole fraction and the distance between the flamefronts.

For ϕ_{CH}=0.6 (Figure 3d), the experimental NO profile, obtained only at 0.3MPa, is shifted to the right compared to the calculated ones. The two mechanisms are in the error bars and give similar results. In this latter case for the leanest flame, the important shift of the flame from the bottom burner could be attributed to stabilisation problems but the maximum NO mole fraction is well predicted.

Figure 4 compares the experimental and calculated maximum NO mole fraction for ϕ_{CH}=0.74, ϕ_{CH}=0.7 and ϕ_{CH}=0.65 as a function of pressure.

For ϕ_{CH}=0.74 (Figure 4a), the experimental maximum NO mole fraction slightly increases with pressure from 11.5±2.3 ppm at 0.1 MPa to 15.2±3.1 ppm at 0.7 MPa. Both mechanisms also predict a slight increase of XNO_{max}.

For ϕ_{CH}=0.7 (Figure 4b), the experimental maximum NO mole fraction slightly increases with pressure except at 0.5 MPa where the value is significantly lower. Both mechanisms predict a slight increase of XNO_{max} when pressures increases. At 0.1 and 0.7 MPa, both mechanisms are in reasonable agreement with experiments (within the error bars), however a slight overprediction is observed at 0.3 MPa. Both mechanisms overpredict the lower experimental value observed at 0.5 MPa.

For ϕ_{CH}=0.65 (Figure 4c), Klippenstein predicts an almost constant value of XNO_{max} for the three pressures and GDFkin®3.0_NOmecha2.0 a slight increase with pressure. The experimental maximum NO mole fraction is correctly predicted at 0.1MPa but overestimated at 0.3 MPa and underpredicted at 0.5 MPa by both mechanisms.

This comparison shows that GDFkin®3.0_NOmecha2.0 and Klippenstein mechanisms are able to predict NO mole fraction in our CH_4/H_2/air flames at high pressure, except in certain conditions (ϕ_{CH}=0.7 at 0.5 MPa and ϕ_{CH}=0.65 at 0.3 MPa).

4.3. Effects of hydrogen addition

As shown in Table 1, adding hydrogen in the methane flame (for the same equivalence ratio, i.e. ϕ_C=0.7) tends to increase the adiabatic temperature. For instance, at 0.1 MPa, the value of the adiabatic temperature in CH_4/air flame at ϕ_C=0.7 is 1841 K whereas it is 1909 K in the CH_4/H_2/air flame. In order to study the effect of hydrogen addition on NO profiles, Figure 5 compares the experimental profiles obtained in the CH_4/air and CH_4/H_2/air flames for the same equivalence ratio relative to methane ϕ_C=0.7 for pressure ranging from 0.1 to 0.7 MPa. It shows that the effect of hydrogen addition is an increase of the amount of NO produced in the flames for all pressures. This can be explained by the increase of the adiabatic temperature as mentioned above. Moreover, the distance between the flamefronts is increased when hydrogen is added (due to higher laminar flame velocity, as shown in Table 1).

Figure 6 shows the evolution of the calculated and experimental maximum NO mole fractions obtained with the two mechanisms with and without hydrogen addition in the flames. It shows, as mentioned above, that hydrogen addition (20% H_2 in CH_4/H_2 mixture) induces an increase of the NO mole fraction by roughly a factor of 2 . This trend is satisfactorily estimated by both mechanisms as well as the evolution as a function of pressure.

This experimental and numerical study shows that the effect of hydrogen addition is to increase the NO concentration as the flame temperature increases (same equivalence ratio). Nevertheless, the main advantage for the addition of hydrogen is to allow stabilisation of leaner flames for which the amount of NO produced is lower. This is shown in Figure 7, which represents the experimental maximum NO mole fractions as a function of the equivalence ratio

for pressure ranging from 0.1 MPa to 0.7MPa. For instance, at 0.5 MPa, it is thus possible to reduce the amount of NO by a factor of 3.5 from 14 ppm for ϕ_{CH}=0.7 to 4 ppm for ϕ_{CH}=0.61.

4.4. Kinetic analysis

A kinetic analysis, carried out to compare the GDFkin®3.0_NOmecha2.0 and Klippenstein mechanisms, based on the rates of production and consumption as a function of the distance from the bottom burner, was performed. The comparison of NO formation sub-mechanisms (prompt, thermal, NNH and N_2O) in the GDFkin®3.0_NOmecha2.0 and Klippenstein mechanisms has already been carried out in a previous publication [35]. As mentioned above, the thermal and NNH mechanisms are identical in both reaction mechanisms. The N_2O mechanism is identical in terms of reactions but not in terms of rate constants and significant differences have been noted for the prompt-NO formation mechanism and subsequent NCN chemistry.

Figure 8 shows the net rates of consumption of N_2 in terms of percentages for all the conditions studied in this paper (the procedure was already detailed in [35, 40]. This is thus possible to understand how the NO precursor, i.e. N_2, decomposes through the four main pathways: prompt, thermal, NNH and N_2O.

For ϕ_{CH}=0.74 (Figure 8a), at atmospheric pressure, all the four pathways contribute significantly to the formation of NO for both mechanisms, contributions are as follow: N_2O>prompt>thermal>NNH for GDFkin®3.0_NOmecha2.0 and thermal>NNH>N_2O>prompt for Klippenstein. The contribution of the prompt and N_2O pathways are slightly higher for GDFkin®3.0_NOmecha2.0 compared to Klippenstein, and the contributions of NNH and thermal are slightly lower. When pressure increases, both mechanisms agree with an increase of the N_2O pathway and decrease of the NNH route. However, for the prompt pathway, Klippenstein presents a decrease of its contribution as pressure increases, as

GDFkin®3.0_NOmecha2.0 presents a very slight increase. For the thermal route, Klippenstein predicts an increase of its contribution with pressure raise as GDFkin®3.0_NOmecha2.0 predicts a slight decrease between 0.1 and 0.3 MPa and then a slight increase when the pressure is further increases to 0.5 and 0.7 MPa.

For ϕ_{CH}=0.7 (Figure 8b), at atmospheric pressure, again all the four pathways contribute significantly to the formation of NO for both mechanisms, contributions are as follow: N_2O>prompt>thermal>NNH for GDFkin®3.0_NOmecha2.0 and N_2O>NNH>thermal>prompt for Klippenstein. As for ϕ_{CH}=0.74, when pressure increases, both mechanisms agree with an increase of the N_2O pathway and decrease of the NNH route. For prompt pathway, a decrease is observed for Klippenstein and a slight increase for GDFkin®3.0_NOmecha2.0. Concerning the thermal route, a slight increase is predicted by Klippenstein as GDFkin®3.0_NOmecha2.0 presents the same trends as for ϕ_{CH}=0.74 (slight decrease between 0.1 and 0.3 MPa and slight increase at 0.5 and 0.7 MPa).

For ϕ_{CH}=0.65 (Figure 8c), the N_2O pathway becomes predominant for both mechanisms, the NNH pathway decreases with pressure raise. For the thermal and prompt, the differences observed between the two mechanisms are equivalent than for ϕ_{CH}=0.74 and 0.7.

For the ϕ_{CH}=0.6 (Figure 8d), the N_2O contribution is roughly 80% for both mechanisms, the main difference is observed for the prompt pathway (higher contribution for GDFkin®3.0_NOmecha2.0).

The net rates of consumption of N_2 were also compared in the case at ϕ_C=0.7 with and without hydrogen [see 35, 40]. The result of this comparison is given in Figure 9 for both mechanisms. Figure 9a shows that according to the GDFkin®3.0_NOmecha2.0 mechanism, the addition of hydrogen at any pressure leads to an increase of the thermal contribution (in the range of 8-9%), a decrease of the N_2O pathway (in the range of 10%), a very slight decrease of the prompt pathway (in the range of 1-3%). For the NNH pathway, at atmospheric pressure, its contribution

increases from 16.5 to 21.1% when hydrogen is added, and only weak variations (~1%) are observed at higher pressures. The Klippenstein mechanism (Figure 9b) predicts, whatever the pressure, that the addition of hydrogen leads to a slight increase in the contribution of the prompt-NO pathway (in the range of 3-4%) and the NNH pathway (2-3%), a significant increase in the contribution of the thermal pathway and a significant decrease of the N_2O route. The main differences observed in this analysis concerns the relative contributions of the prompt and thermal pathways between the two mechanisms, GDFkin®3.0_NOmecha2.0 systematically predicts a higher contribution of the prompt pathway and a lower contribution of the thermal pathway compared to Klippenstein. A sensitivity analysis was carried out on the different flames to highlight the reactions that are important in the presence of hydrogen. Figure 10 shows the results of this sensitivity analysis only for reactions containing nitrogen species. All the results of the sensitivity analyses are presented in Table A in the supplementary file.

The sensitivity analysis presented in Figure 10a (ϕ_{CH}=0.74) shows that the same reactions appear sensitive in both mechanisms with the exception of the $N_2O+O \rightarrow 2NO$ reaction which only appears with a positive sensitivity coefficient in the Klippenstein mechanism at 0.1 and 0.3 MPa. The sensitivity of this reaction decreases with pressure. The same quantitative trends are observed in both mechanisms for the following reactions: $N_2+O+M \rightarrow N_2O+M$, $N_2+O \rightarrow N+NO$, $N_2O+H \rightarrow NH+NO$ and $N_2O+H \rightarrow N_2+OH$, with sensitivity coefficients decreasing with increasing pressure. The reactions $N_2+H \rightarrow NNH$ and $NNH \rightarrow N_2+H$ appear sensitive only at 0.1 MPa for both mechanisms. Concerning the prompt-NO initiation reaction, the $CH+N_2 \rightarrow NCN+H$ reaction, it appears sensitive in the Klippenstein mechanism only at atmospheric pressure. In the GDFkin®3.0_NOmecha2.0 mechanism, this reaction has a sensitivity that decreases with pressure raise.

Figure 10b presents the results of the sensitivity analysis for ϕ_{CH}=0.70 for the two reaction mechanisms. The same quantitative trends, namely a decrease in sensitivity with pressure raise,

are observed in both mechanisms for the following reactions: $N_2+O+M \rightarrow N_2O+M$, $N_2+O \rightarrow N+NO$, $N_2O+H \rightarrow NH+NO$ and $N_2O+H \rightarrow N_2+OH$. The reaction $N_2+H \rightarrow NNH$ is only sensitive at 0.1 MPa for both mechanisms but the reverse reaction $NNH \rightarrow N_2+H$ only occurs in the Klippenstein mechanism at atmospheric pressure, and the $N_2O+O \rightarrow 2NO$ reaction only in the GDFkin®3.0_NOmecha2.0 mechanism at atmospheric pressure. For this condition, the same observation can be made as for ϕ_{CH}=0.74 for the initiation reaction of prompt-NO: it is only sensitive at 0.1 MPa in the Klippenstein mechanism, and its sensitivity decreases with pressure raise in the GDFkin®3.0_NOmecha2.0 mechanism.

For ϕ_{CH}=0.65 (Figure 10c), the $N_2+O+M \rightarrow N_2O+M$, $N_2O+H \rightarrow NH+NO$, $N_2O+O \rightarrow 2NO$ and $N_2O+H \rightarrow N_2+OH$ reactions show similar behaviours in both mechanisms (sensitivity coefficients that decrease with pressure raise). Differences are observed for the reaction of thermal-NO ($N_2+O \rightarrow N+NO$) which only occurs at atmospheric pressure in GDFkin®3.0_NOmecha2.0 mechanism and only at 0.1 and 0.3 MPa in Klippenstein mechanism. Here again, the same observation can be made for the initiation reaction of prompt-NO. The $NNH+O \rightarrow NH+NO$ only appears for Klippenstein at 0.1 MPa.

Finally, for the condition ϕ_{CH}=0.60 (Figure 10d), the same reactions with similar sensitivity coefficients appear in both mechanisms, except for the $N_2O+M \rightarrow N_2+O+M$ reaction which appears only in the Klippenstein mechanism.

In order to complete the study on the effect of hydrogen carried out previously in paragraph 4.3, it is possible to compare the NO sensitivity analyses with (this paper) and without [35] hydrogen addition in the methane/air flames at ϕ_C=0.7 for both mechanisms. For reactions containing only N-species, in the case of GDFkin®3.0_NOmecha2.0, similar results are observed quantitatively for the reactions: $N_2+O+M \rightarrow N_2O+M$, $N_2O+H \rightarrow NH+NO$, $CH+N_2 \rightarrow NCN+H$ and $N_2O+H \rightarrow N_2+OH$. The NNH pathway reaction ($NNH \leftrightarrows N_2+H$) do not

appear in the NO sensitivity analysis performed in the methane/air flame, but it appears when H_2 is added. In the case of the Klippenstein mechanism, the sensitivity analyses with and without hydrogen are similar for reactions containing nitrogen species.

5. Conclusion

In the present work, new experimental results of NO profile measurements by LIF in laminar counterflow lean methane/hydrogen/air flames stabilised from atmospheric (0.1MPa) to high pressure (0.7 MPa) were obtained. H_2 content was fixed at 20% in the fuel and the equivalence ratio was progressively decreased from 0.74 to 0.6.

Experimental NO mole fraction profiles in 12 flames were presented and the effects of hydrogen addition, equivalence ratio and pressure on NO concentration were discussed. In general, the increase in pressure induces an increase in NO concentration, a decrease in equivalence ratio results in a decrease in NO concentration, and the addition of hydrogen (20% H_2-80%CH_4) has the effect of doubling the NO concentration.

These results were compared to the simulations using two detailed mechanisms: GDF®kin3.0_NOmecha2.0 and the mechanism from Klippenstein et al., which are the most recent high-pressure NOx formation mechanisms available in the literature.

Overall, a good agreement between experiments and modelling was observed (profile shape and maximum NO mole fraction) and both mechanisms are able to predict the effects of pressure, equivalence ratio and H_2 addition.

A kinetic analysis based on ROP/ROC of NO and sensitivity analyses was performed in all the flame conditions for both mechanisms to highlight the main reactions that lead to the formation and consumption of NO. In all the conditions and for both mechanisms, the preponderance of the N_2O pathway to the formation of NO emerges.

The addition of hydrogen modifies the contribution of the different NO-formation pathways, especially a decrease of the N_2O pathway and an increase of the thermal pathway contributions due to an increase in flame temperature.

Acknowledgements

This work was supported by the ANR program BLAN-08-0130(NO-Mecha). The authors thank the French Ministère de l'Enseignement Supérieur et de la Recherche, the Hauts de France Region, the Centre Region and the European Fund for Regional Economic Development for their financial support of this project. The authors also want to warmly thank Luc-Sy Tran for his help in using the software Logesoft.

List of references

[1] S. D. Emami, R. Md. Kasmani, M.D. Hamid, C.R.C. Hassan, K.M. Mokhtar, Kinetic and dynamic analysis of hydrogen-enrichment mixtures in combustor systems – A review paper, Renewable and Sustainable Energy Reviews 62 (2016) 1072-1082.

[2] Y. Yu, G. Vanhove, J.F. Griffiths, S. De Ferrières, and J.-F. Pauwels, Influence of EGR and syngas components on the autoignition of natural gas in a rapid compression machine: a detailed experimental study, Energy Fuels 27 (2013) 3988-3996.

[3] H. Guo, G.J. Smallwood, F. Liu, Y. Ju, O.L. Gülder, The effect of hydrogen addition on flammability limit and NOx emission in ultra-lean counterflow CH_4/air premixed flames. Proc. Combust. Inst. 30 (2005) 303-311.

[4] A. Genovese, N. Contrisciani, F. Ortenzi, V. Cazzola, On road experimental tests of hydrogen/natural gas blends on transit buses, Int. J. Hydrogen Energy 36 (2011) 1775-1783.

[5] B. Riddel., Malmö hydrogen and CNG/Hydrogen filling station and Hythane bus project, In WHEC 16, 13-16 June 2006, Lyon France.

[6] A. Villante, A. Genovese, Hydromethane: A bridge towards the hydrogen economy or an unsustainable promise?, Int. J. Hydrogen Energy 37 (2012) 11541-11548.

[7] T. Boushaki, Y. Dhué, L. Selle, B. Ferret, T. Poinsot, Effects of hydrogen and steam addition on laminar burning velocity of methane/air premixed flame: Experimental and numerical analysis, Int. J. of Hydrogen Energy 37 (2012) 9412-9422.

[8] J.L. Gauducheau, B. Denet, G. Searby, A numerical study of lean CH_4/H_2/air premixed flames at high pressure, Combust. Sci. Tech. 137 (1998) 81-99.

[9] C.T. Bowman, R.K. Hanson, D.F. Davidson, W.C. Gardiner, V.V. Lissianski, G.P. Smith, D.M. Golden, M. Frenklach and M. Goldenberg, GRImech2.11, http://www.me.berkeley.edu/gri_mech/

[10] G.J. Rortveit, K. Zepter, O. Skreiberg, M. Fossum, J.E. Hustad., A comparison of low-NOx burners for combustion of methane and hydrogen mixtures, Proc. Combust. Inst. 29 (2002) 1123-1129.

[11] E.R. Hawkes, J.H. Chen, Direct numerical simulation of hydrogen-enriched lean premixed methane-air flames, Combust. Flame 138 (2004) 242-258.

[12] S. Naha, S.K. Aggarwal, Fuel effects on NOx emissions in partially premixed flames. Combust. Flame 139 (2004) 90-105.

[13] G.P. Smith, D.M. Golden, M. Frenklach, N.W. Moriarty, B. Eiteneer, M. Goldenberg, C.T. Bowman., R.K. Hanson, S. Song, W.C. Gardiner, V.V. Lissianski and Z. Qin, GRImech3.0, http://www.me.berkeley.edu/gri_mech/

[14] F.H.V. Coppens, J. De Ruyck, A.A. Konnov, The effects of composition on burning velocity and nitric oxide formation in laminar premixed flames of CH_4+H_2+O_2+N_2, Combust. Flame 149 (2007) 409-417.

[15] F.H.V. Coppens, J. De Ruyck, A.A. Konnov, Effects of hydrogen enrichment on adiabatic burning velocity and NO formation in methane+air flames, Exp. Th. And Fluid Sci. 31 (2007) 437-444.

[16] S. De Ferrières, A. El Bakali, B. Lefort, M. Montero, J.-F. Pauwels, Experimental and numerical investigation of low-pressure laminar premixed synthetic natural gas /O_2/N_2 and natural gas/H_2/O_2/N_2 flames, Combust. Flame 154 (2008) 601-623.

[17] J. Biet, J.L Delfau, L. Pillier, C. Vovelle, Influence of CO_2 and H_2 on the chemical structure of a premixed, lean methane-air flame, Proc. of the European Combustion Meeting 2007, Chania, Crete, April 11-13 2007.

[18] A. Parente, C. Galletti, L. Tognotti, Effect of the combustion model and kinetic mechanism on the MILD combustion in an industrial burner fed with hydrogen enriched fuels, Int. J. Hydrogen Energy 33 (2008) 7553-7564.

[19] C. Galletti, A. Parente, M. Derudi, R. Rota, L. Tognotti, Numerical and experimental analysis of NO emissions from a lab-scale burner fed with hydrogen-enriched fuels and operating in MILD combustion, Int. J. Hydrogen Energy 34 (2009) 8339-8351.

[20] A. Mardani, S. Tabejamaat, NO_x Formation in H_2-CH_4 Blended Flame Under MILD Conditions, Combust. Sci. Tech. 184 (2012) 995-1010.

[21] X. Gao, F. Duan, S.C. Lim, M.S. Yip, NOx formation in hydrogen-methane turbulent diffusion flame under the moderate or intense low-oxygen dilution conditions, Energy 59 (2013) 559-569.

[22] E. Hu, Z. Huang, J. He, H. Miao, Experimental and numerical study on laminar burning velocities and flame instabilities of hydrogen-air mixtures at elevated pressures and temperatures, Int. J. of hydrogen Energy 34 (2009) 8741-8755.

[23] J. Wang, Z. Huang, C. Tang, H. Miao, X. Wang, Numerical study of the effect of hydrogen addition on methane-air mixtures combustion, Int. J. of Hydrogen Energy 34 (2009) 1084-1096.

[24] A.V. Sepman, A.V. Mokhov, H.B. Levinsky, Extending the predictions of chemical mechanisms for hydrogen combustion: Comparison of predicted and measured flame temperatures in burner-stabilized, 1-D flames, Int. J. of Hydrogen Energy 36 (2011) 9298-9303.

[25] P. Zahedi and K. Yousefi, Effects of pressure and carbon dioxide, hydrogen and nitrogen concentration on laminar burning velocities and NO formation of methane–air mixtures, Journal of Mechanical Science and Technology 28 (2014) 377-386.

[26] Y. Ying, D. Liu, Detailed influences of chemical effects of hydrogen as fuel additive on methane flame, Int. J. of Hydrogen Energy 40 (2015) 3777-3788.

[27] Z.L. Wei, C.W. Leung, C.S. Cheung, Z.H. Huang, Effects of equivalence ratio, H_2 and CO_2 addition on the heat release characteristics of premixed laminar biogas-hydrogen flame, Int. J. of Hydrogen Energy 41 (2016) 6567-6580.

[28] Z.L. Wei, H.S. Zhen, C.W. Leung, C.S. Cheung, Z.H. Huang, Experimental and numerical study on the emission characteristics of laminar premixed biogas-hydrogen impinging flame, Fuel 195 (2017) 1-11.

[29] Z. Riahi, H. Bounaouara, I. Hraiech, M.A. Mergheni, J.-C. Sautet, S. B. Nasrallah, Combustion with mixed enrichment of oxygen and hydrogen in lean regime, Int. J. Hydrogen Energy 42 (2017) 8870-8880.

[30] M.J. Acero, L.E. Pacheco, C.A. Diaz, Numerical Study of the Effect of Hydrogen Addition On the Laminar Flame Speed and Premixed Flame Structure of Biogas, International Journal of Renewable Energy Research 8 (2018) 1098-1104.

[31] L.V. Moskaleva and M.C. Lin, The Spin-Conserved Reaction CH + N_2 → H + NCN: A Major Pathway to Prompt NO Studied by Quantum/Statistical Theory Calculations and Kinetic Modeling of Rate Constant, Proc. Combust. Inst. 28 (2000) 2393-2401.

[32] V. Vasudevan, R.K. Hanson, C.T. Bowman, D.M. Golden and D.F. Davidson, Shock tube study of the reaction of CH with N_2: overall rate and product branching, J. Phys. Chem. A 111 (2007) 11818-11830.

[33] N. Lamoureux, H. El Merhubi, L. Pillier, S. de Persis, P. Desgroux, Modeling of NO formation in low pressure premixed flames, Combust. Flame 163 (2016) 557-575.

[34] A. El Bakali, P. Dagaut, L. Pillier, P. Desgroux, J-F. Pauwels, A. Rida and P. Meunier, Experimental and modeling study of the oxidation of natural gas in a premixed flame, shock tube, and jet-stirred reactor, Combust. Flame 137 (2004) 109-128.

[35] S. de Persis, L. Pillier, M. Idir, J. Molet, N. Lamoureux, P. Desgroux, NO formation in high pressure premixed flames: experimental results and validation of a new revised reaction mechanism, Fuel, submitted.

[36] S.J. Klippensetin, M. Pfeifle, A.W. Jasper, P. Glarborg, Theory and modelling of relevance to prompt-NO formation at high pressure, Combust. Flame 195 (2018) 3-17.

[37] LOGERESEARCH, http://logesoft.com/loge-software/, LOGE AB, 2017

[38] A. Matynia, M. Idir, J. Molet, C. Roche, S. de Persis and L. Pillier, Absolute OH concentration profiles measurements in high pressure counterflow flames by coupling LIF, PLIF and absorption techniques, Appl. Phys. B 108 (2012) 393-405.

[39] A. Matynia, J. Molet, C. Roche, M. Idir, S. de Persis and L. Pillier, Measurement of OH concentration profiles by laser diagnostics and modelling in high pressure counter-flow premixed methane-air and biogas-air flames, Combust. Flame 159 (2012) 3300-3311.

[40] L. Pillier, M. Idir, J. Molet, A. Matynia, S. de Persis, Experimental study and modelling of NOx formation in high pressure counter-flow premixed CH_4/air flames, Fuel 150 (2015) 394-407.

[41] Y.B. Zeldovich, The oxidation of nitrogen in combustion and explosions, Acta Physicochimica 21 (1946) 577-68.

[42] C.P. Fenimore, Formation of nitric oxide in premixed hydrocarbon flames, Symp. (Int.) Combust. 13 (1971) 373-379.

[43] J.W. Bozzelli and A.M. Dean, O + NNH: A possible new route for NOx formation in flames. Int. J. Chem. Kin. 27 (1995) 1097-1109.

[44] P.C. Malte and D.T. Pratt, The role of energy-releasing kinetics in NOx formation: fuel-lean, jet-stirred CO-Air combustion, Combust. Sci. and Tech. 9 (1974) 221-231.

List of table captions

Table 1. *CH_4/H_2/air counterflow premixed flame conditions (XCH_4 is the mole fraction of methane, XH_2 is the mole fraction of hydrogen, XO_2 is the mole fraction of oxygen, and XN_2 is the mole fraction of nitrogen); Air dilution ratio is used.*

Table 2. *Rate constants for the reactions involved in the prompt-NO sub-mechanism and NCN chemistry, the thermal-NO initiation, the NNH pathway and the N_2O pathway for the GDFkin®3.0_NOmecha2.0 and Klippenstein mechanisms.*

List of tables

Table 1

	ϕ_{CH}/ϕ_C	Pressure (MPa)	T_o(K)[a]	XCH_4[a]	XH_2[a]	XO_2[a]	XN_2[a]	Total flowrate[a] (NL/min)	Free flame calculation[b]	
									Adiabatic flame temperature T_f, K	Laminar burning velocity S_L, cm.s^{-1} (T_0=300K)
CH_4/ air flames	0.7	0.1	303	0.0685	0	0.1952	0.7363	1.57	1841	16.7
		0.3	313					2.50	1849	10.3
		0.5	323					2.97	1857	7.9
		0.7	323					4.01	1857	6.5
CH_4/H_2/air flames	0.74/0.7	0.1	303	0.0672	0.0171	0.1922	0.7235	1.86	1909	23.0
		0.3	313					3.71	1944	14.7
		0.5	323					4.29	1947	11.5
		0.7	323					4.96	1945	9.6
	0.7/0.66	0.1	303	0.0638	0.0159	0.1933	0.7269	1.58	1852	19.5
		0.3	313					2.79	1876	12.2
		0.5	323					3.47	1880	9.3
		0.7	323					3.99	1878	7.7
	0.65/0.61	0.1	303	0.0592	0.0148	0.1945	0.7315	1.26	1770	15.0
		0.3	313					2.02	1785	8.9
		0.5	323					2.62	1789	6.5
	0.6/0.57	0.3	313	0.0555	0.0139	0.1952	0.7354	1.51	1712	6.4

[a]*Experimental conditions for the bottom burner, in standard conditions, i.e. T=273K and P=101325Pa.*

[b]*Flame temperature and laminar burning velocity calculated for a free flame configuration using LOGESOFT [29] and GDFkin®3.0 associated with NOmecha2.0 [27]*

Table 2

Reactions First order: s^{-1} Second order: $cm^3/mol\cdot s$ Third order: $cm^6/mol^2\cdot s$ R = 1.987 cal/mol·K	Rate constant parameters (in Arrhenius form A T^{β} exp (-Ea/RT))	
	GDFkin®3.0_NOmecha2.0	**Klippenstein**
Prompt-NO initiation and NCN consumption		
$CH+N_2 \rightleftharpoons NCN+H$	1.950×10^{12} 0.00 16915	2.500×10^{9} 0.89 16620
$NCN+H \rightleftharpoons HCN+N$	3.839×10^{14} 0.00 7956	2.200×10^{11} 0.71 5321
$NCN+H \rightleftharpoons HNCN$	1.79×10^{42} -9.58 5250	1.500×10^{30} -5.43 4415
$NCN+O_2 \rightleftharpoons NO+NCO$	3.80×10^{9} 0.51 24616	1.300×10^{12} 0.0 23167
$NCN+OH \rightleftharpoons HCN+NO$	4.71×10^{13} 0.44 4006	2.600×10^{8} 1.22 3593
$NCN+O \rightleftharpoons CN+NO$	9.60×10^{13} 0.00 1387	2.500×10^{13} 0.17 -34
$NCN+H_2 \rightleftharpoons HNCN+H$	4.11×10^{13} 0.00 24163	/
$NCN+M \rightleftharpoons C+N_2+M$	8.90×10^{14} 0.00 62127	8.900×10^{14} 0.00 62100
$NCN+NCN \rightleftharpoons 2CN+N_2$	3.70×10^{12} 0.00 0	/
$NCN+C \rightleftharpoons 2CN$	1.00×10^{14} 0.00 0	/
$NCN+N \rightleftharpoons CN+N_2$	1.00×10^{13} 0.00 0	/
$NCN+CN \rightleftharpoons C_2N_2+N$	1.25×10^{14} 0.00 8000	/
$NCN+H \rightleftharpoons HNC+N$	/	4.300×10^{-4} 4.690 2434
$NCN+OH \rightleftharpoons NCNOH$	/	1.800×10^{32} -6.370 3924
$NCN+OH \rightleftharpoons NCO+NH$	/	1.700×10^{18} -1.830 4143
$NCN+NO \rightleftharpoons CN+N_2O$		1.900×10^{12} 0.000 6280
Thermal-NO initiation		
$N_2+O \rightleftharpoons N+NO$	1.000×10^{14} 0.00 75490	$N+NO \rightleftharpoons N_2+O$ 9.400×10^{12} 0.140 0
$N+O_2 \rightleftharpoons NO+O$	6.400×10^{9} 1.00 6280	6.400×10^{9} 1.00 6280
$N+OH \rightleftharpoons NO+H$	3.800×10^{13} 0.00 0	3.800×10^{13} 0.00 0
NNH pathway		
$NNH \rightleftharpoons N_2+H$	1.000×10^{9} 0.00 0	1.000×10^{9} 0.00 0
$NNH+O \rightleftharpoons NH+NO$	5.180×10^{11} 0.38 -409	5.180×10^{11} 0.38 -409
N_2O pathway		
$N_2O+M \rightleftharpoons N_2+O+M$	1.300×10^{12} 0.00 62570 LOW/ 0.4E+15 0.0 56600/ N_2/ 1.7/ O_2/ 1.4/ CO_2/ 3.0 / H_2O / 12.0/	9.900×10^{10} 0.00 57901 LOW/6.0E14 0.0 57444/ N_2/1.7/ O_2/1.4/ H_2O/12.0/
$NH+NO \rightleftharpoons N_2O+H$	1.750×10^{14} -0.351 -244	2.700×10^{15} -0.780 20
$N_2O+O \rightleftharpoons 2NO$	9.200×10^{13} 0.00 27679	9.200×10^{13} 0.00 27679

List of figure captions

Figure 1. *Pictures of the CH_4/H_2/air flames stabilised in this work for the following equivalence ratios: ϕ_{CH}=0.74/ϕ_C=0.7; ϕ_{CH}=0.7/ϕ_C=0.66; ϕ_{CH}=0.65/ϕ_C=0.61; ϕ_{CH}=0.6/ϕ_C=0.57 at: 0.1 MPa (T_0 = 303 K), 0.3 MPa (T_0 = 313 K), 0.5 MPa (T_0 = 323 K) and 0.7 MPa (T_0 = 323 K).*

Figure 2. *Experimental NO mole fraction profiles in ppm for the CH_4/H_2/air flames: a) ϕ_{CH}=0.74 (ϕ_C=0.7) at: 0.1 MPa (T_0 = 303 K), 0.3 MPa (T_0 = 313 K), 0.5 MPa (T_0 = 323 K) and 0.7 MPa (T_0 = 323 K)* ~~*pressures from 0.1 to 0.7 MPa*~~*; b) ϕ_{CH}=0.7 (ϕ_C=0.66) at* ~~*pressures from 0.1 to 0.7 MPa*~~*0.1 MPa (T_0 = 303 K), 0.3 MPa (T_0 = 313 K), 0.5 MPa (T_0 = 323 K) and 0.7 MPa (T_0 = 323 K) ; c) ϕ_{CH}=0.65 (ϕ_C=0.61) at 0.1 MPa (T_0 = 303 K), 0.3 MPa (T_0 = 313 K) and 0.5 MPa (T_0 = 323 K)* ~~*pressures ranging from 0.1 to 0.5 MPa*~~

Figure 3. *Comparison between experimental and calculated NO mole fraction profiles in ppm for the CH_4/H_2/air flames: a) ϕ_{CH}=0.74 (ϕ_C=0.7) at 0.1 MPa (T_0 = 303 K), 0.3 MPa (T_0 = 313 K), 0.5 MPa (T_0 = 323 K) and 0.7 MPa (T_0 = 323 K)* ~~*pressures from 0.1 to 0.7 MPa*~~*; b) ϕ_{CH}=0.7 (ϕ_C=0.66) at 0.1 MPa (T_0 = 303 K), 0.3 MPa (T_0 = 313 K), 0.5 MPa (T_0 = 323 K) and 0.7 MPa (T_0 = 323 K)* ~~*pressures from 0.1 to 0.7 MPa*~~*; c) ϕ_{CH}=0.65 (ϕ_C=0.61) at 0.1 MPa (T_0 = 303 K), 0.3 MPa (T_0 = 313 K) and 0.5 MPa (T_0 = 323 K)* ~~*pressures ranging from 0.1 to 0.5 MPa*~~*; d) ϕ_{CH}=0.6 (ϕ_C=0.57) at 0.3 MPa (T_0=313 K).*

Symbol: experiments; modeling with red line: GDFkin®3.0_NOmecha2.0 and blue dotted line: Klippenstein mechanism.

Figure 4. *Comparison between experimental and calculated maximum NO mole fraction XNO_{max} in ppm for the CH_4/H_2/air flames a) ϕ_{CH}=0.74 (ϕ_C=0.7) at 0.1 MPa (T_0 = 303 K), 0.3 MPa (T_0 = 313 K), 0.5 MPa (T_0 = 323 K) and 0.7 MPa (T_0 = 323 K)* ~~*pressures from 0.1 to 0.7 MPa*~~*; b) ϕ_{CH}=0.7 (ϕ_C=0.66) at 0.1 MPa (T_0 = 303 K), 0.3 MPa (T_0 = 313 K), 0.5 MPa (T_0 = 323 K) and 0.7 MPa (T_0 = 323 K)* ~~*pressures from 0.1 to 0.7 MPa*~~*; c) ϕ_{CH}=0.65 (ϕ_C=0.61) at 0.1 MPa (T_0 = 303 K), 0.3 MPa (T_0 = 313 K) and 0.5 MPa (T_0 = 323 K)* ~~*pressures ranging from 0.1 to 0.5 MPa*~~

Symbol: experiments; modeling with red line: GDFkin®3.0_NOmecha2.0 and blue dotted line: Klippenstein mechanism.

Figure 5. *Experimental NO mole fraction profiles in ppm for CH_4/air* (white diamonds) and CH_4/H_2/air (black diamonds) flames as a function of the distance from the bottom burner (in cm) for ϕ_C=0.7 ($\phi_{CH=}$0.74) at 0.1 MPa (T_0 = 303 K), 0.3 MPa (T_0 = 313 K), 0.5 MPa (T_0 = 323 K) and 0.7 MPa (T_0 = 323 K)* ~~*pressures from 0.1 to 0.7 MP*~~*a.*

**the corresponding results are taken from reference [32]*

Figure 6. *Comparison between experimental and calculated maximum NO mole fraction XNO_{max} in ppm for the CH_4/air* and CH_4/H_2/air flames for ϕ_C=0.7 ($\phi_{CH=}$0.74) at 0.1 MPa (T_0 = 303 K), 0.3 MPa (T_0 = 313 K), 0.5 MPa (T_0 = 323 K) and 0.7 MPa (T_0 = 323 K)* ~~*pressures from 0.1 to 0.7 MPa*~~*.*

Symbol: experiments; modeling with red line: GDFkin®3.0_NOmecha2.0 and blue dotted line: Klippenstein mechanism.

**the corresponding results are taken from reference [32]*

Figure 7. *Experimental maximum NO mole fraction XNO_{max} in ppm for the CH_4/H_2/air flames as a function of equivalence ratio ϕ_{CH}/ϕ_C ($\phi_{CH=}0.74/\phi_C=0.7/$; $\phi_{CH}=0.7/\phi_C=0.66$; $\phi_{CH}=0.65/\phi_C=0.61$; $\phi_{CH}=0.6/\phi_C=0.5$) at: 0.1 MPa (T_0=303K) in blue, 0.3 MPa (T_0=313K) in red; 0.5 MPa (T_0=323K) in green and 0.7 MPa (T_0=323 K) in purple.*

Figure 8. *Relative contribution (in %) of the four NO formation pathways obtained from N_2 consumption rates: a) $\phi_C=0.7$ ($\phi_{CH=}0.74$) at 0.1 MPa (T_0 = 303 K), 0.3 MPa (T_0 = 313 K), 0.5 MPa (T_0 = 323 K) and 0.7 MPa (T_0 = 323 K)* ~~*pressures from 0.1 to 0.7 MPa*~~*; b) $\phi_C=0.66$ ($\phi_{CH}=0.7$) at 0.1 MPa (T_0 = 303 K), 0.3 MPa (T_0 = 313 K), 0.5 MPa (T_0 = 323 K) and 0.7 MPa (T_0 = 323 K)*~~*pressures from 0.1 to 0.7 MPa*~~*; c) $\phi_C=0.61$ ($\phi_{CH}=0.65$) at 0.1 MPa (T_0 = 303 K), 0.3 MPa (T_0 = 313 K) and 0.5 MPa (T_0 = 323 K)* ~~*pressures ranging from 0.1 to 0.5 MPa*~~*; d) $\phi_C=0.57$ ($\phi_{CH}=0.6$) at 0.3 MPa T_0 = 313 K); for GDFkin®3.0_NOmecha2.0 (in red) and Klippenstein mechanism (in blue).*

Figure 9. *Relative contribution of the four NO formation pathways obtained from N_2 consumption rates, with and without H_2 addition at $\phi_C=0.7$ ($\phi_{CH=}0.74$), at 0.1 MPa (T_0 = 303 K), 0.3 MPa (T_0 = 313 K), 0.5 MPa (T_0 = 323 K) and 0.7 MPa (T_0 = 323 K)* ~~*pressures from 0.1 to 0.7 MPa*~~*; a) for GDFkin®3.0_NOmecha2.0 and b) for Klippenstein mechanism.*

Figure 10. *Normalized sensitivity coefficients of NO to reaction rate coefficients (only N-species containing reactions are considered): a) $\phi_C=0.7$ ($\phi_{CH=}0.74$); b) $\phi_C=0.66$ ($\phi_{CH}=0.7$); c) $\phi_C=0.61$ ($\phi_{CH}=0.65$); d) $\phi_C=0.57$ ($\phi_{CH}=0.6$) at 0.3 MPa, as a function of pressure (0.1 MPa and T_0=303 K in black, 0.3MPa and T_0=303 K in red, 0.5MPa and T_0=323 K in blue, 0.7MPa and T_0=323 K in green), for GDFkin®3.0_NOmecha2.0 (left column) and Klippenstein mechanism (right column).*

List of figures

Figure 1

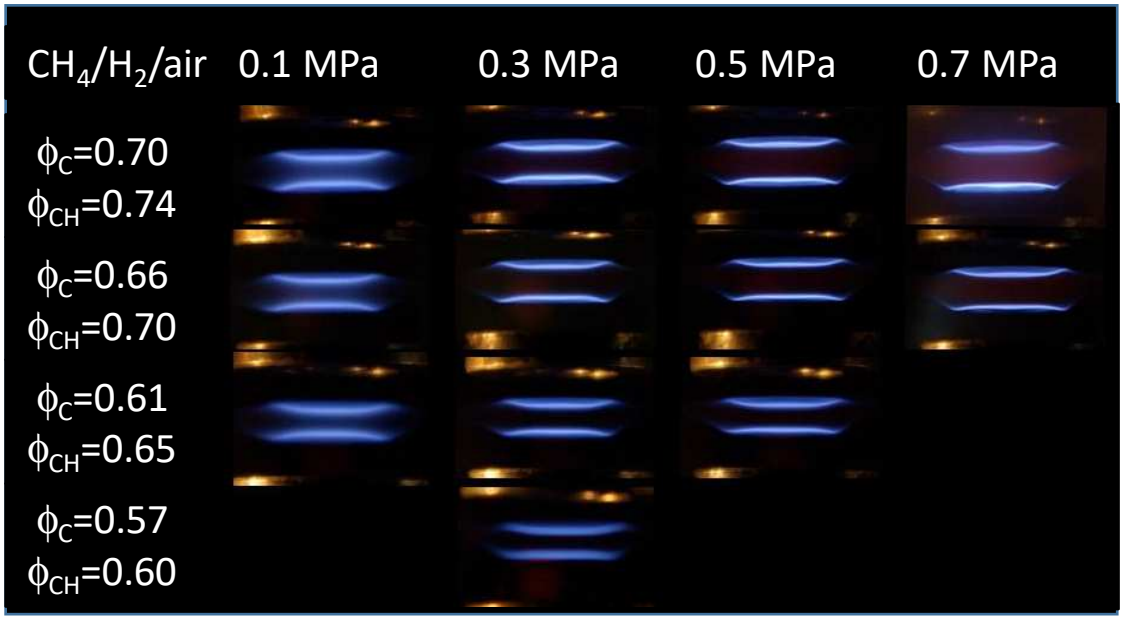

Figure 2

a)

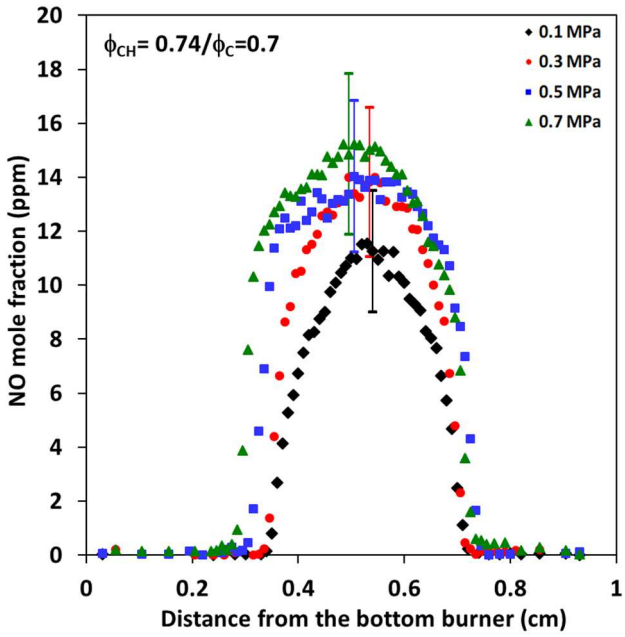
ϕ_{CH}= 0.74/ϕ_C=0.7
0.1 MPa
0.3 MPa
0.5 MPa
0.7 MPa
NO mole fraction (ppm)
Distance from the bottom burner (cm)
0
2
4
6
8
10
12
14
16
18
20
0
0.2
0.4
0.6
0.8
1

b)

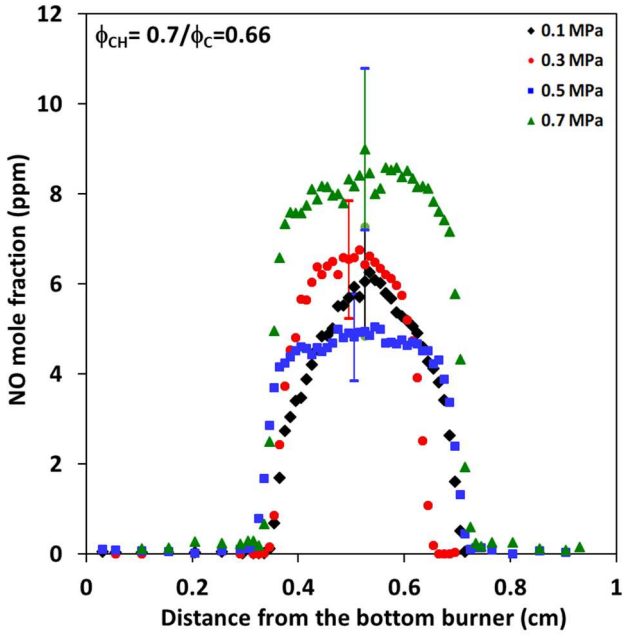
ϕ_{CH}= 0.7/ϕ_C=0.66
0.1 MPa
0.3 MPa
0.5 MPa
0.7 MPa
NO mole fraction (ppm)
Distance from the bottom burner (cm)
0
2
4
6
8
10
12
0
0.2
0.4
0.6
0.8
1

c)

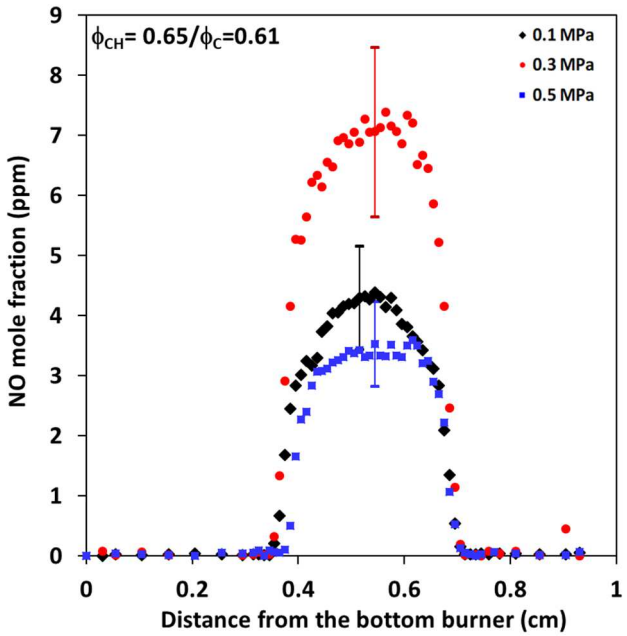
ϕ_{CH}= 0.65/ϕ_C=0.61
0.1 MPa
0.3 MPa
0.5 MPa
NO mole fraction (ppm)
Distance from the bottom burner (cm)
0
1
2
3
4
5
6
7
8
9
0
0.2
0.4
0.6
0.8
1

Figure 3

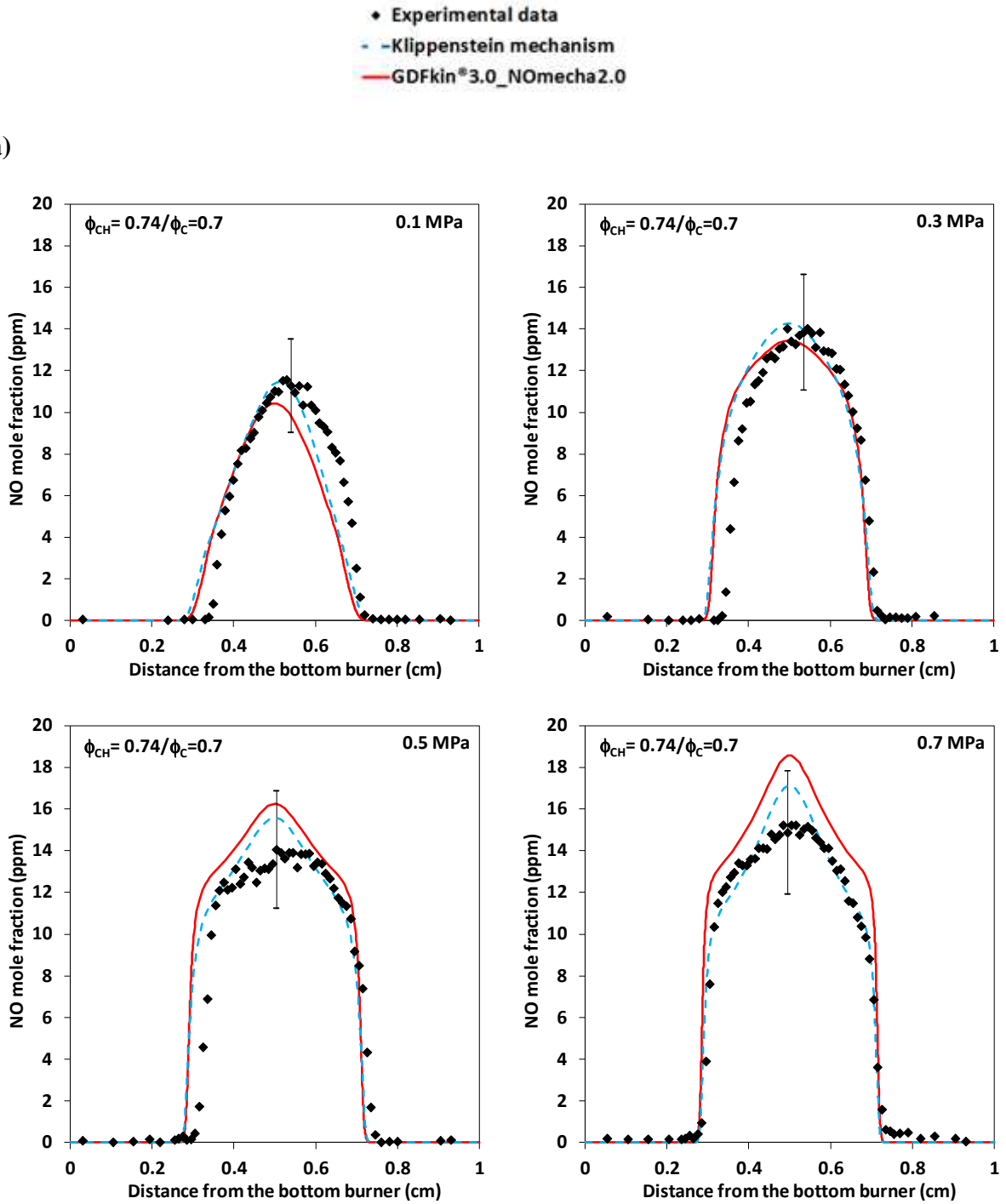
Experimental data
-Klippenstein mechanism
GDFkin®3.0_NOmecha2.0
a)
ϕ_{CH}= 0.74/ϕ_C=0.7
0.1 MPa
0.3 MPa
0.5 MPa
0.7 MPa
NO mole fraction (ppm)
Distance from the bottom burner (cm)
0
2
4
6
8
10
12
14
16
18
20
0.2
0.4
0.6
0.8
1

b)

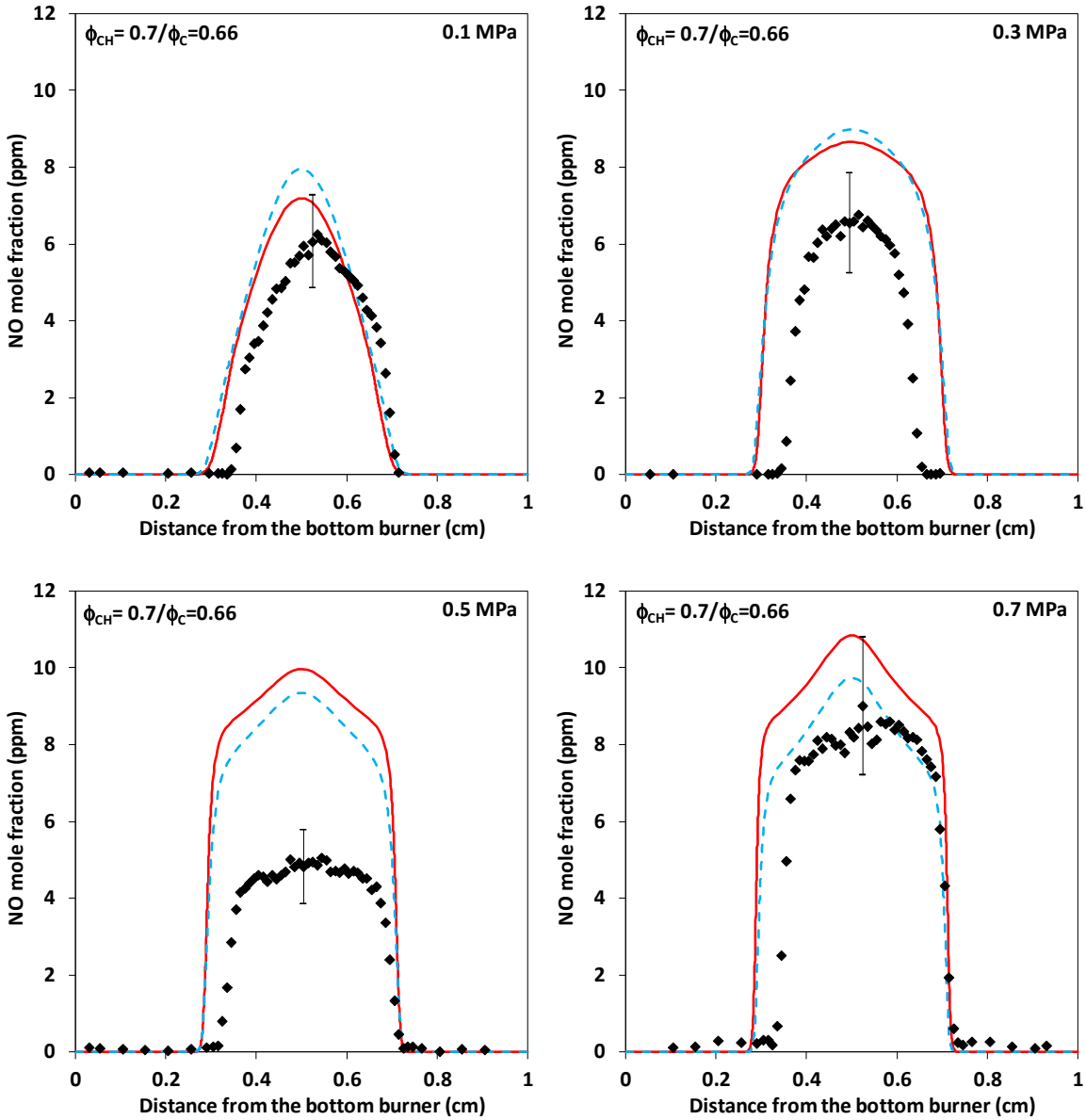
ϕ_{CH}= 0.7/ϕ_C=0.66
0.1 MPa
0.3 MPa
0.5 MPa
0.7 MPa
NO mole fraction (ppm)
Distance from the bottom burner (cm)
0
2
4
6
8
10
12
0.2
0.4
0.6
0.8
1

c)

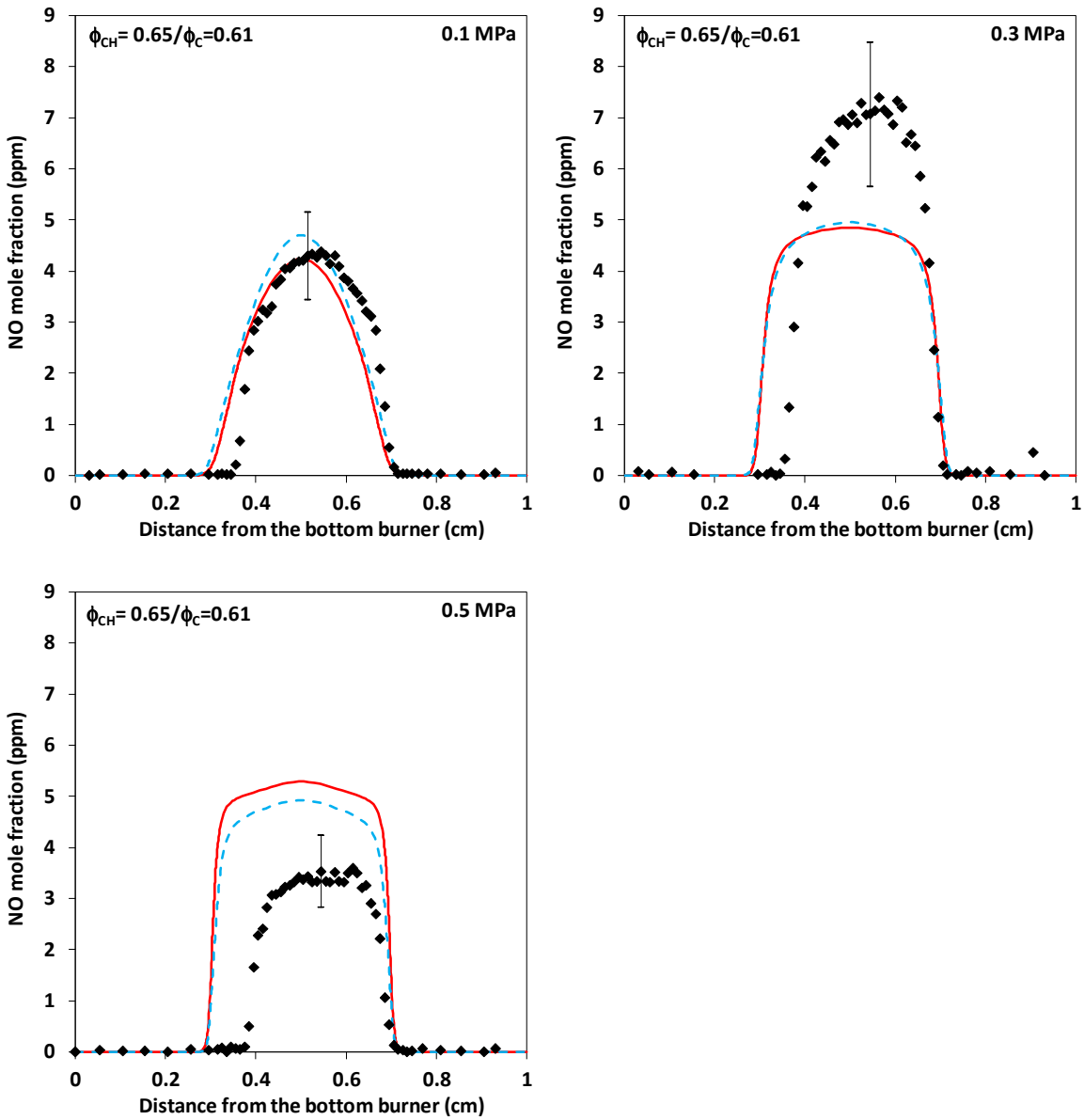
ϕ_{CH}= 0.65/ϕ_C=0.61
0.1 MPa
0.3 MPa
0.5 MPa
NO mole fraction (ppm)
Distance from the bottom burner (cm)
0
1
2
3
4
5
6
7
8
9
0.2
0.4
0.6
0.8
1

d)

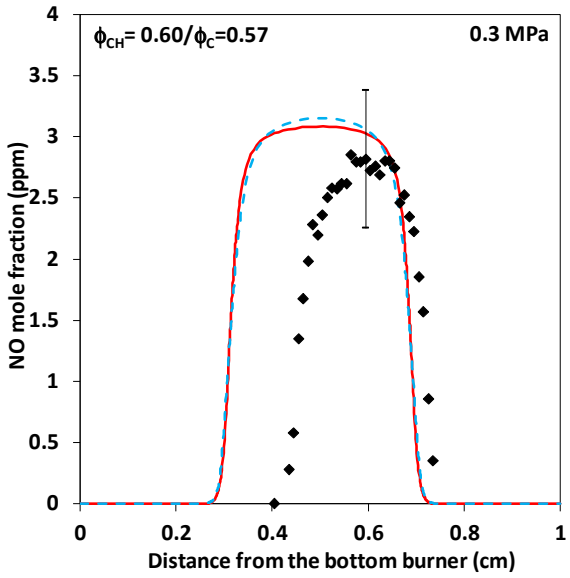
ϕ_{CH}= 0.60/ϕ_C=0.57
0.3 MPa
NO mole fraction (ppm)
Distance from the bottom burner (cm)
0
0.5
1
1.5
2
2.5
3
3.5
4
0
0.2
0.4
0.6
0.8
1

Figure 4

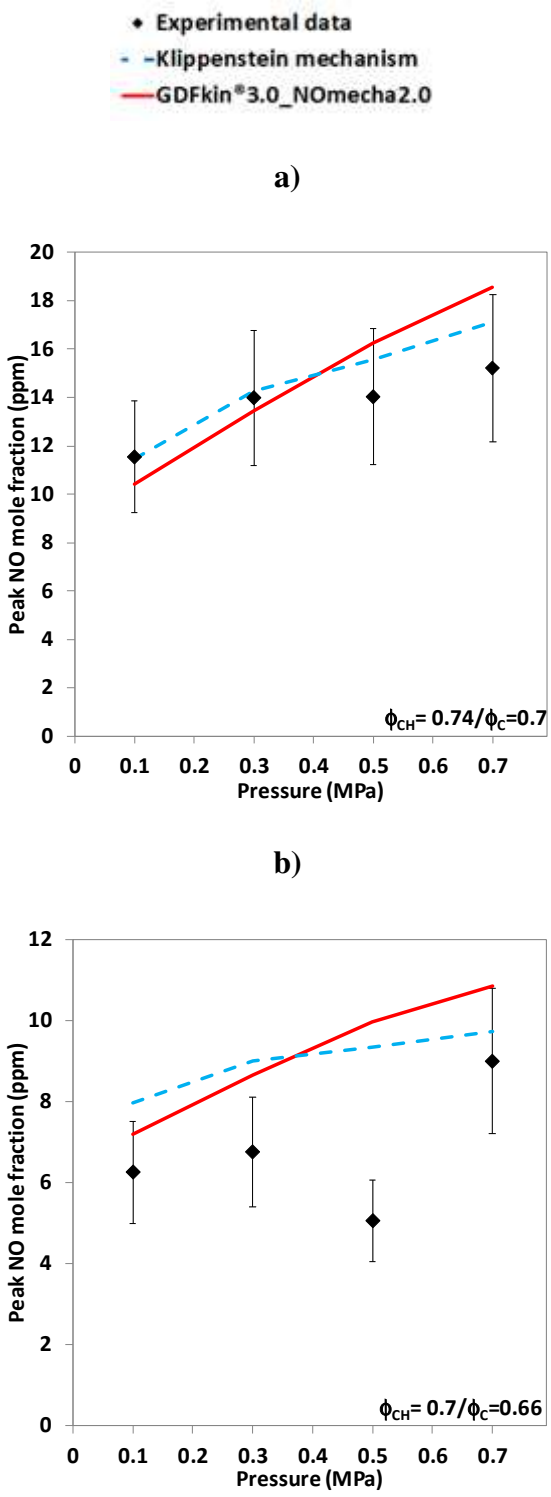
Experimental data
Klippenstein mechanism
GDFkin®3.0_NOmecha2.0
a)
Peak NO mole fraction (ppm)
Pressure (MPa)
ϕ_{CH}= 0.74/ϕ_C=0.7
b)
Peak NO mole fraction (ppm)
Pressure (MPa)
ϕ_{CH}= 0.7/ϕ_C=0.66

c)

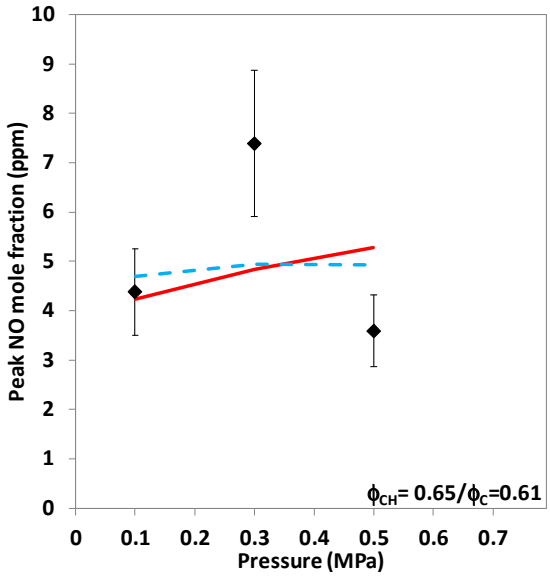
Peak NO mole fraction (ppm)
10
9
8
7
6
5
4
3
2
1
0
0
0.1
0.2
0.3
0.4
0.5
0.6
0.7
Pressure (MPa)
ϕ_{CH}= 0.65/ϕ_C=0.61

Figure 5

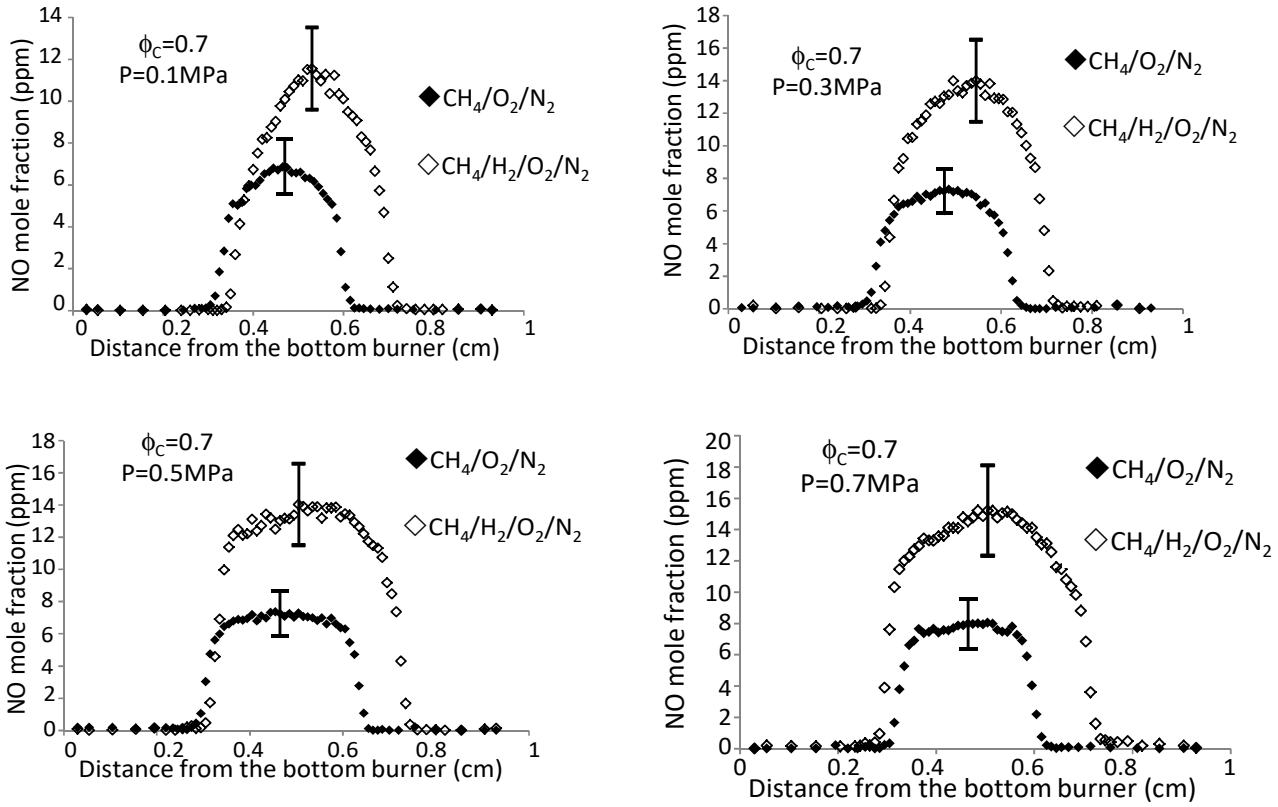
ϕC=0.7
P=0.1MPa
CH4/O2/N2
CH4/H2/O2/N2
NO mole fraction (ppm)
Distance from the bottom burner (cm)
ϕC=0.7
P=0.3MPa
CH4/O2/N2
CH4/H2/O2/N2
NO mole fraction (ppm)
Distance from the bottom burner (cm)
ϕC=0.7
P=0.5MPa
CH4/O2/N2
CH4/H2/O2/N2
NO mole fraction (ppm)
Distance from the bottom burner (cm)
ϕC=0.7
P=0.7MPa
CH4/O2/N2
CH4/H2/O2/N2
NO mole fraction (ppm)
Distance from the bottom burner (cm)

Figure 6

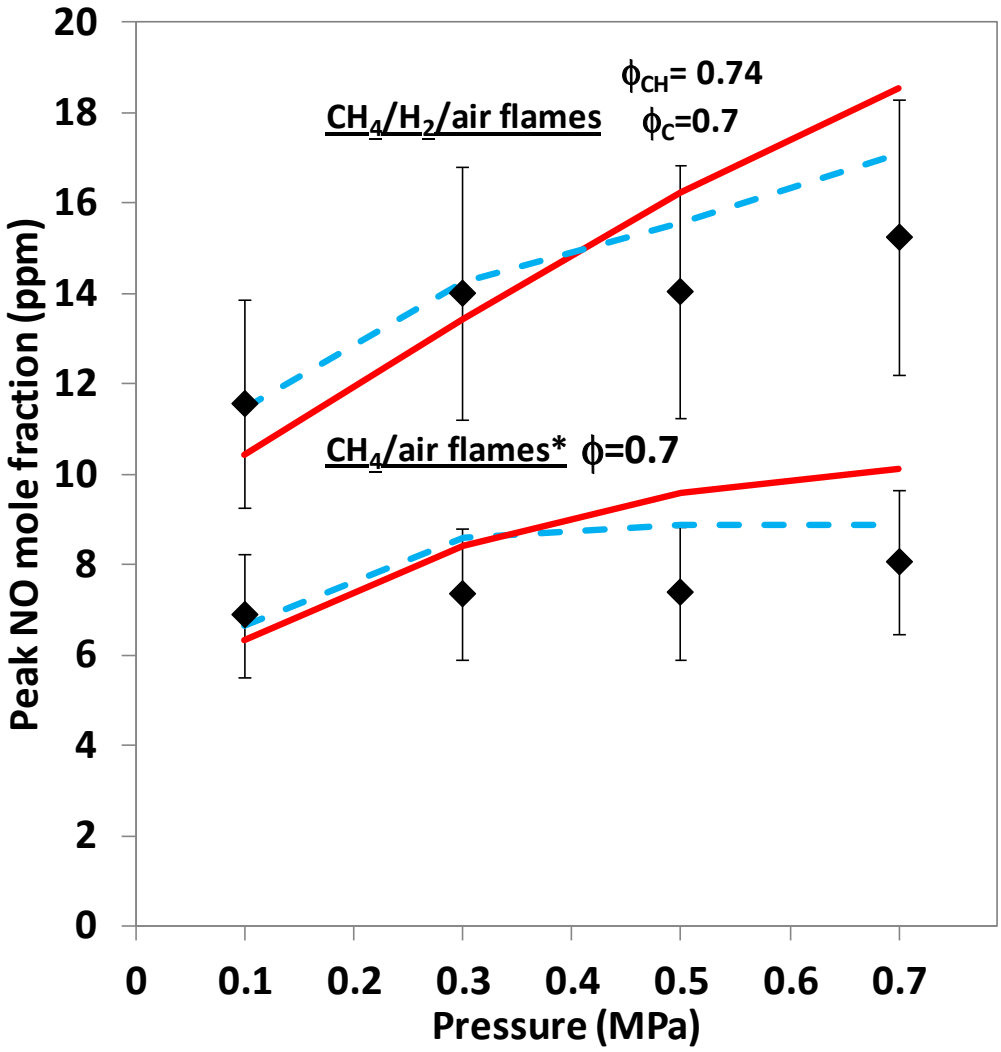
20
18
16
14
12
10
8
6
4
2
0
Peak NO mole fraction (ppm)
0
0.1
0.2
0.3
0.4
0.5
0.6
0.7
Pressure (MPa)
CH4/H2/air flames
ϕCH= 0.74
ϕC=0.7
CH4/air flames* ϕ=0.7

Figure 7

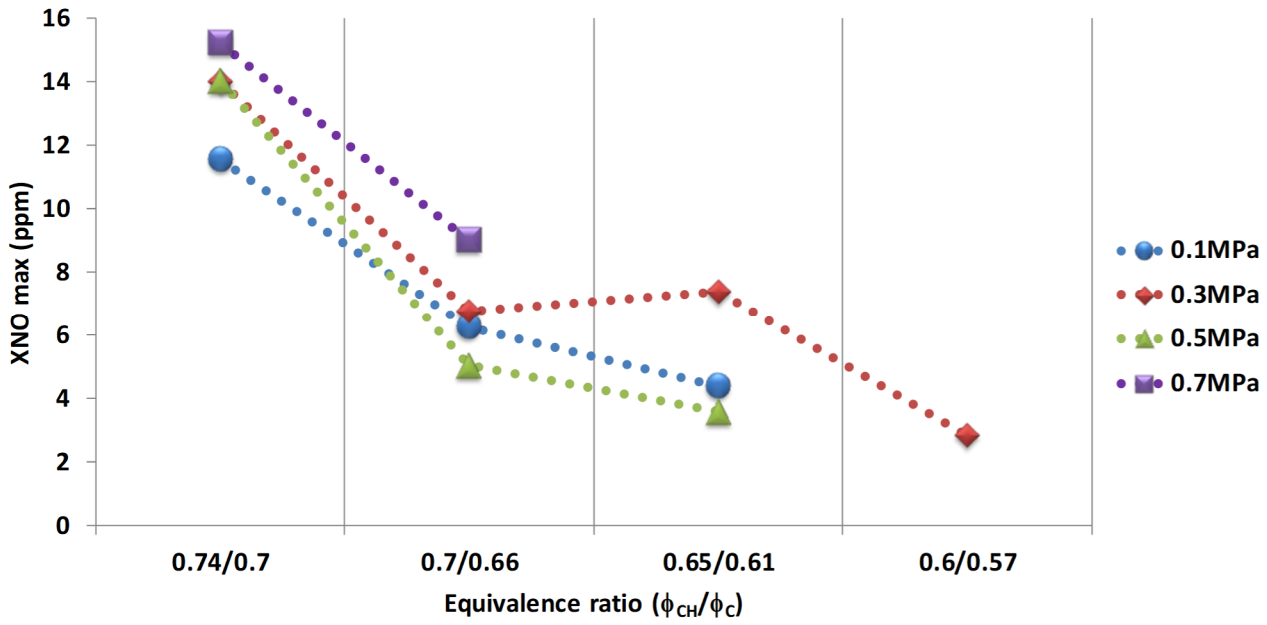
16
14
12
10
8
6
4
2
0
XNO max (ppm)
0.74/0.7
0.7/0.66
0.65/0.61
0.6/0.57
Equivalence ratio (ϕ_{CH}/ϕ_C)
0.1MPa
0.3MPa
0.5MPa
0.7MPa

Figure 8

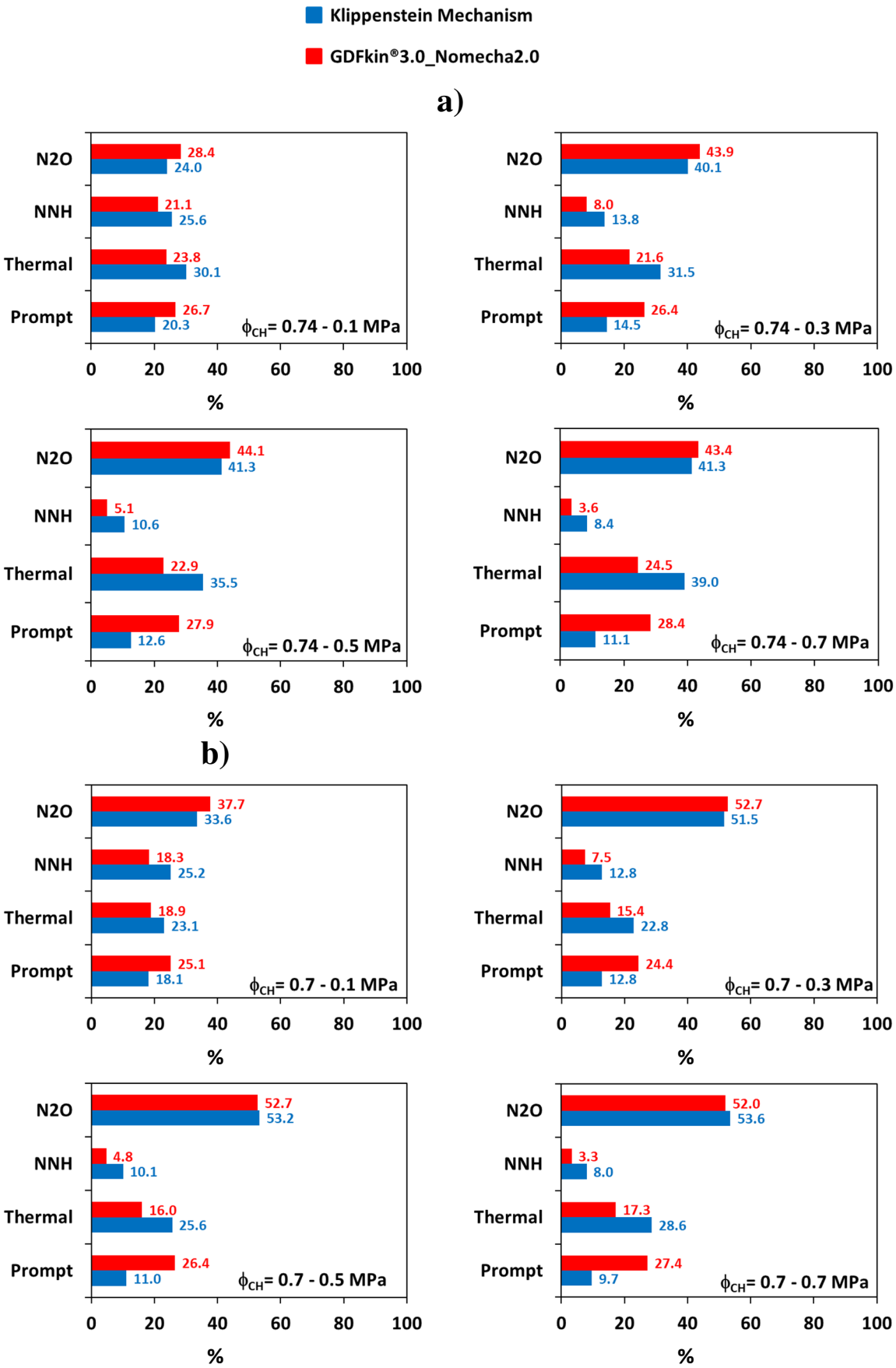
Klippenstein Mechanism
GDFkin®3.0_Nomecha2.0
a)
N2O
NNH
Thermal
Prompt
28.4
24.0
21.1
25.6
23.8
30.1
26.7
20.3
ϕCH= 0.74 - 0.1 MPa
43.9
40.1
8.0
13.8
21.6
31.5
26.4
14.5
ϕCH= 0.74 - 0.3 MPa
44.1
41.3
5.1
10.6
22.9
35.5
27.9
12.6
ϕCH= 0.74 - 0.5 MPa
43.4
41.3
3.6
8.4
24.5
39.0
28.4
11.1
ϕCH= 0.74 - 0.7 MPa
b)
37.7
33.6
18.3
25.2
18.9
23.1
25.1
18.1
ϕCH= 0.7 - 0.1 MPa
52.7
51.5
7.5
12.8
15.4
22.8
24.4
12.8
ϕCH= 0.7 - 0.3 MPa
52.7
53.2
4.8
10.1
16.0
25.6
26.4
11.0
ϕCH= 0.7 - 0.5 MPa
52.0
53.6
3.3
8.0
17.3
28.6
27.4
9.7
ϕCH= 0.7 - 0.7 MPa
0
20
40
60
80
100
%

c)

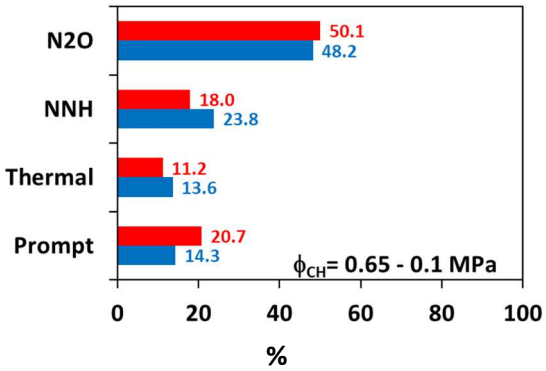
N2O
NNH
Thermal
Prompt
50.1
48.2
18.0
23.8
11.2
13.6
20.7
14.3
ϕCH= 0.65 - 0.1 MPa
0
20
40
60
80
100
%

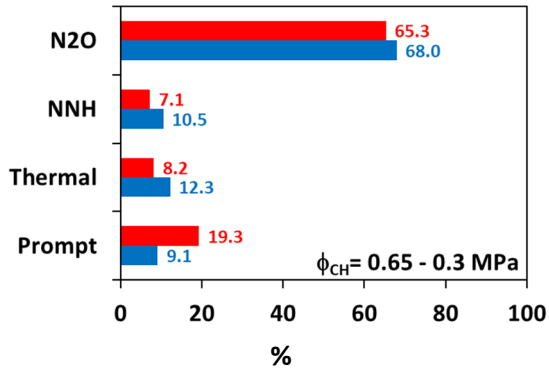
N2O
NNH
Thermal
Prompt
65.3
68.0
7.1
10.5
8.2
12.3
19.3
9.1
ϕCH= 0.65 - 0.3 MPa
0
20
40
60
80
100
%

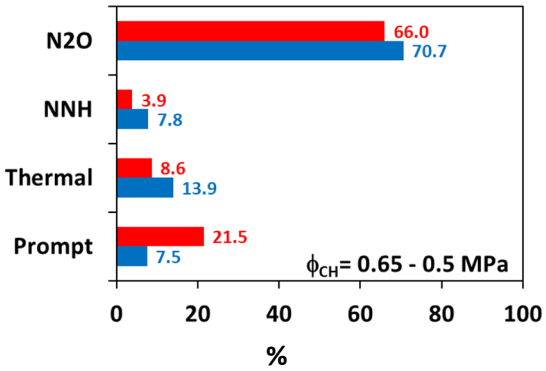
N2O
NNH
Thermal
Prompt
66.0
70.7
3.9
7.8
8.6
13.9
21.5
7.5
ϕCH= 0.65 - 0.5 MPa
0
20
40
60
80
100
%

d)

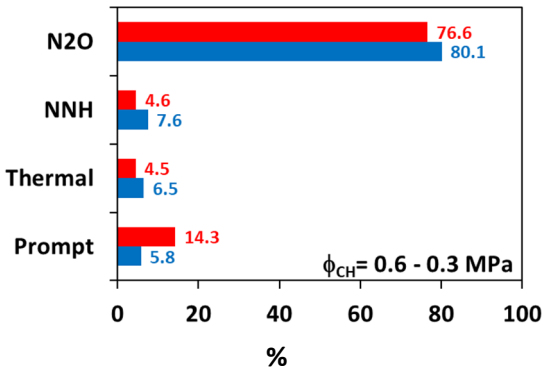
N2O
NNH
Thermal
Prompt
76.6
80.1
4.6
7.6
4.5
6.5
14.3
5.8
ϕCH= 0.6 - 0.3 MPa
0
20
40
60
80
100
%

Figure 9

a) GDFkin®3.0_NOmecha20

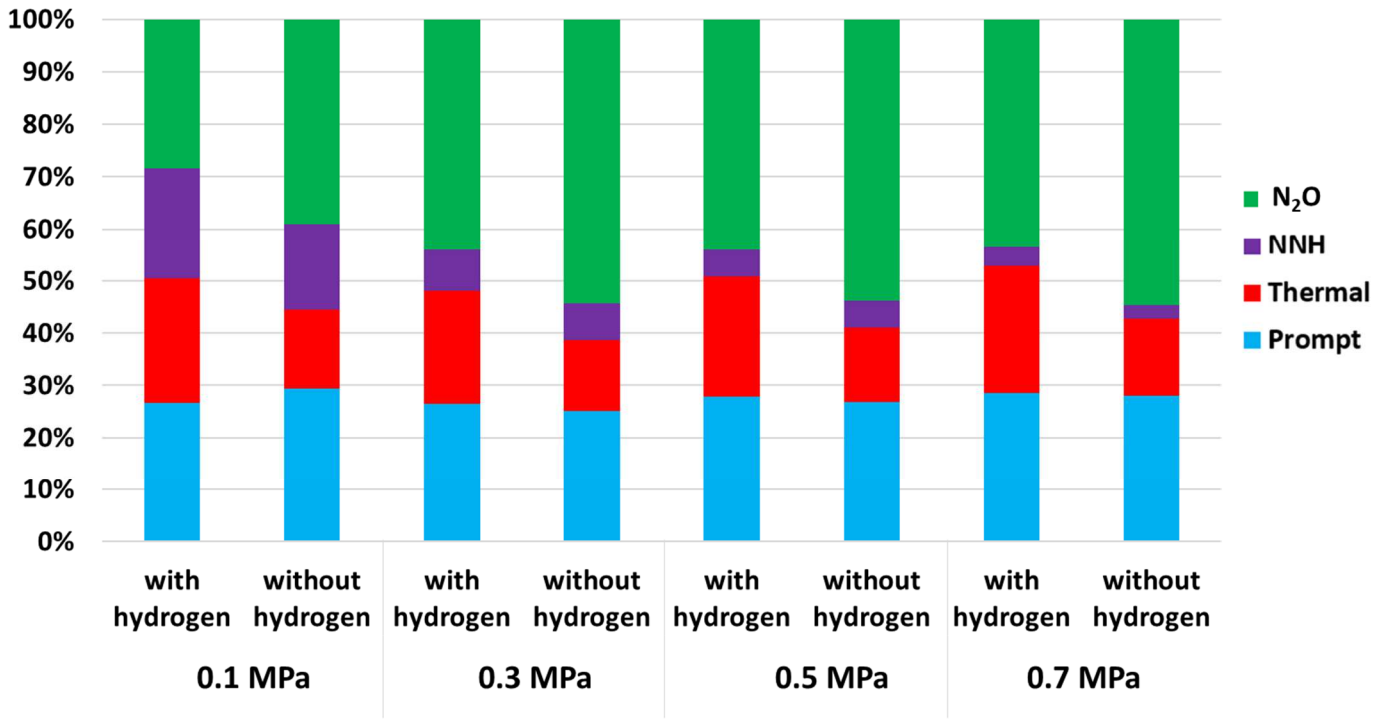

b) Klippenstein

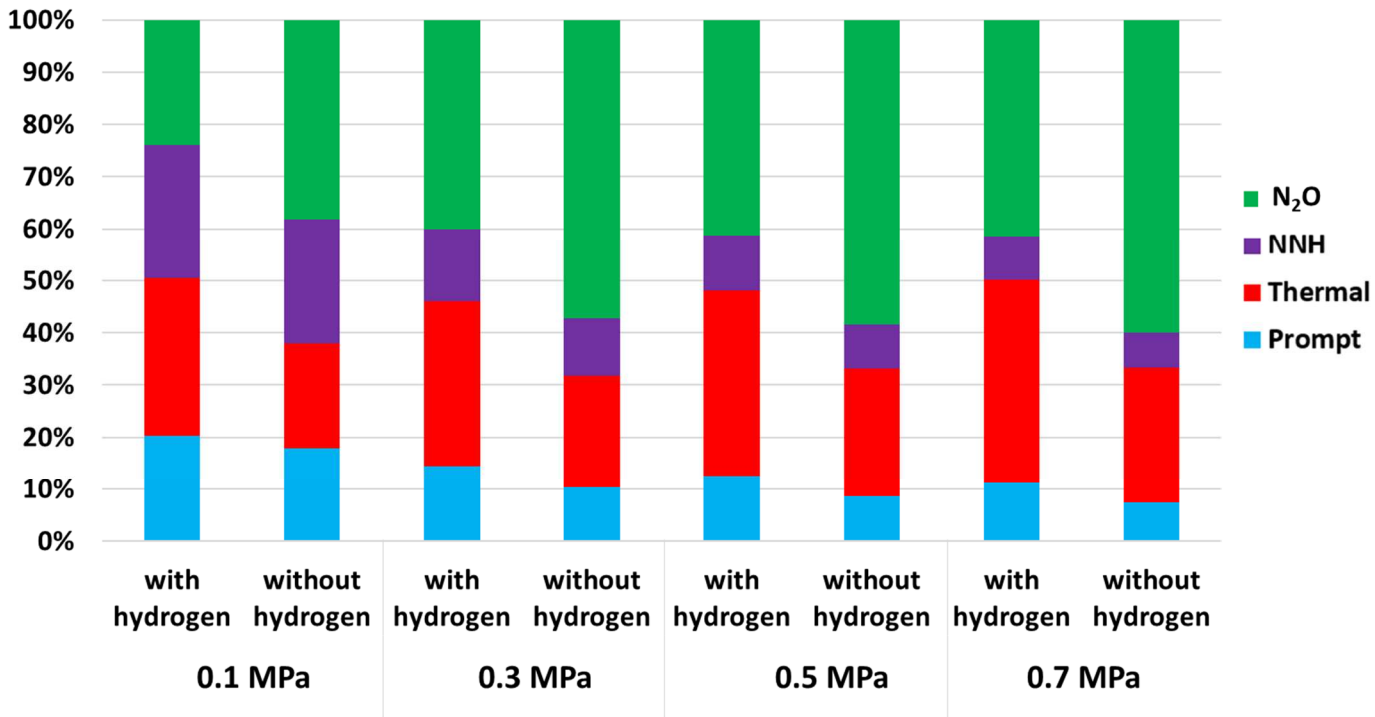

Figure 10

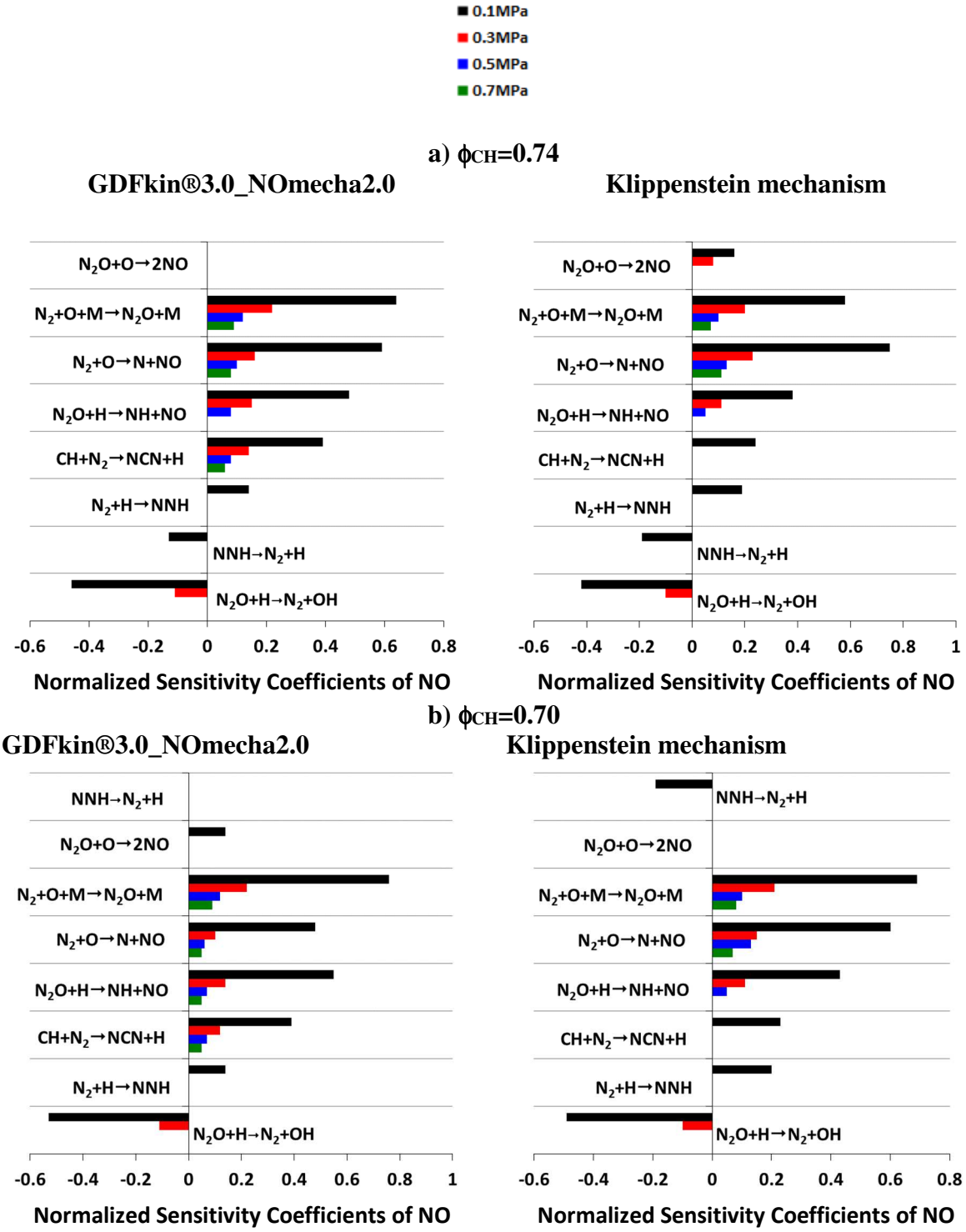
0.1MPa
0.3MPa
0.5MPa
0.7MPa
a) ϕCH=0.74
GDFkin®3.0_NOmecha2.0
Klippenstein mechanism
N2O+O→2NO
N2+O+M→N2O+M
N2+O→N+NO
N2O+H→NH+NO
CH+N2→NCN+H
N2+H→NNH
NNH→N2+H
N2O+H→N2+OH
-0.6 -0.4 -0.2 0 0.2 0.4 0.6 0.8
-0.6 -0.4 -0.2 0 0.2 0.4 0.6 0.8 1
Normalized Sensitivity Coefficients of NO
Normalized Sensitivity Coefficients of NO
b) ϕCH=0.70
GDFkin®3.0_NOmecha2.0
Klippenstein mechanism
NNH→N2+H
N2O+O→2NO
N2+O+M→N2O+M
N2+O→N+NO
N2O+H→NH+NO
CH+N2→NCN+H
N2+H→NNH
N2O+H→N2+OH
-0.6 -0.4 -0.2 0 0.2 0.4 0.6 0.8 1
-0.6 -0.4 -0.2 0 0.2 0.4 0.6 0.8
Normalized Sensitivity Coefficients of NO
Normalized Sensitivity Coefficients of NO

c) ϕ_{CH}=0.65

GDFkin®3.0_NOmecha2.0

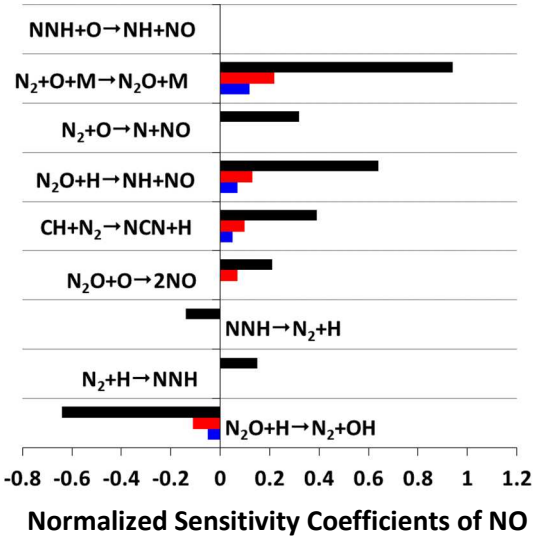

Klippenstein mechanism

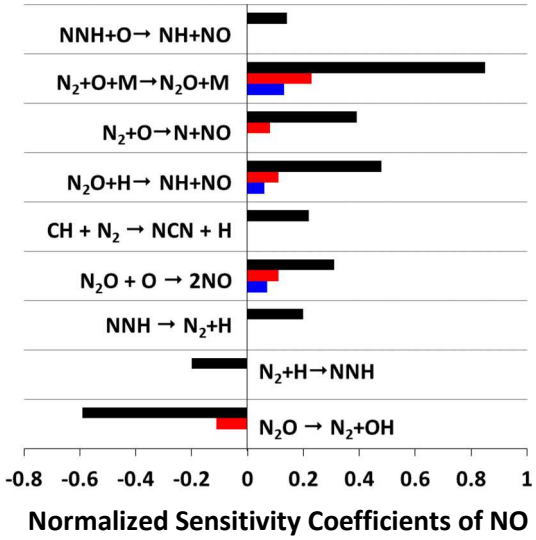

Normalized Sensitivity Coefficients of NO

d) ϕ_{CH}=0.60

GDFkin®3.0_NOmecha2.0

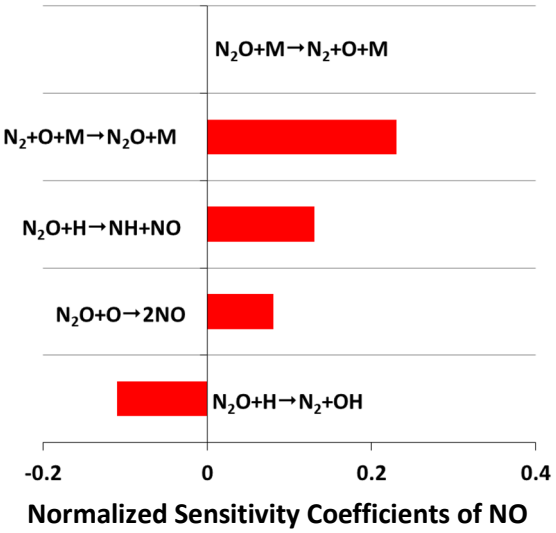

Klippenstein mechanism

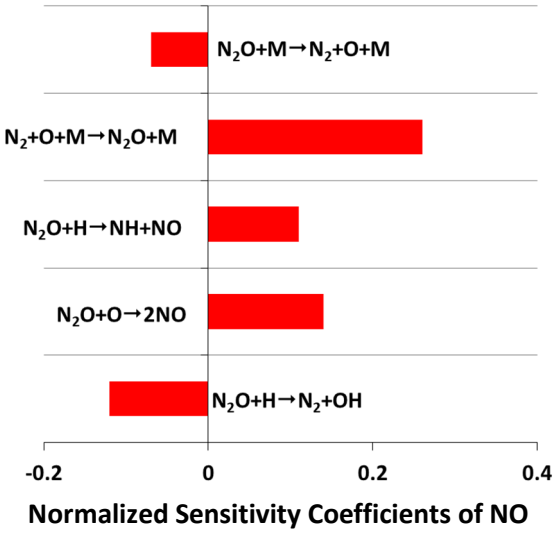

Supplementary file

Figure A

Comparison between calculated temperature profiles obtained with the two mechanisms (red solid line: GDFkin®3.0 with NOmecha2.0 [27], blue dotted line: Klippenstein mechanism [28]) assuming the adiabatic hypothesis for CH_4/H_2/air flames: a) ϕ_C=0.7 (ϕ_{CH}=0.74) at pressures from 0.1 to 0.7 MPa; b) ϕ_C=0.66 (ϕ_{CH}=0.7) at pressures from 0.1 to 0.7 MPa; c) ϕ_C=0.61 (ϕ_{CH}=0.65) at pressures ranging from 0.1 to 0.5 MPa; d) ϕ_C=0.57 (ϕ_{CH}=0.6) at 0.3 MPa.

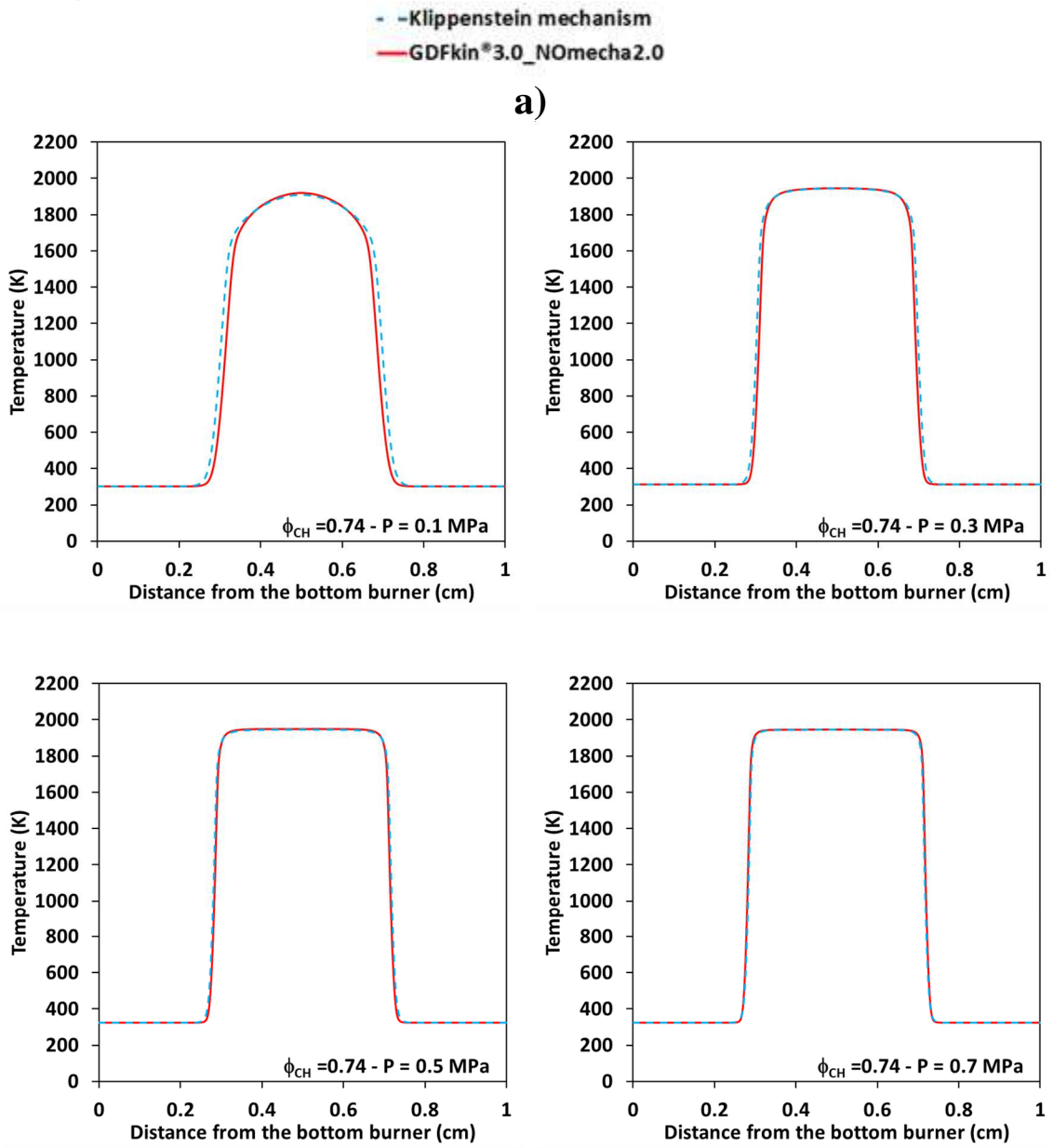

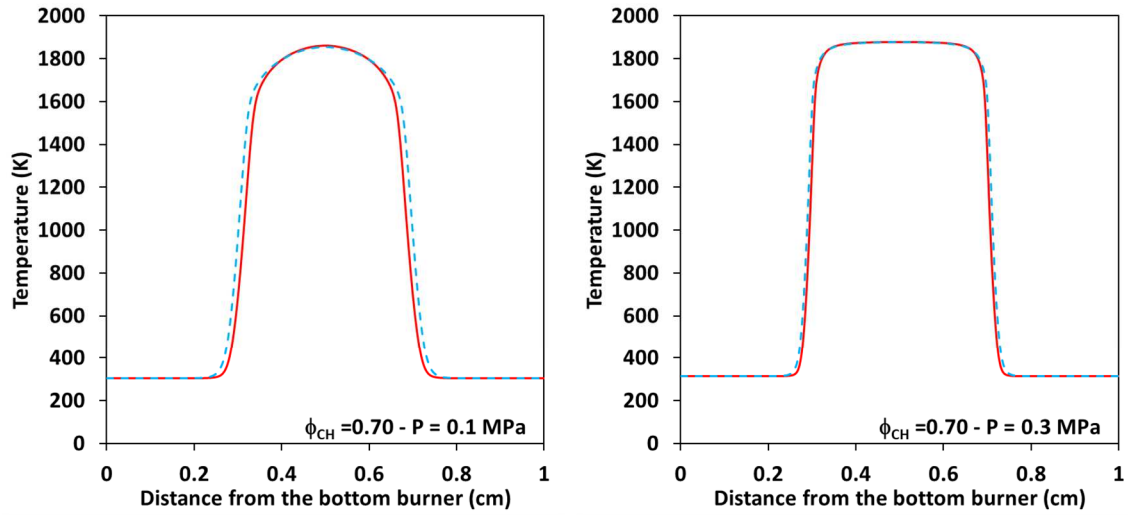
Temperature (K)
Distance from the bottom burner (cm)
ϕ_{CH} =0.70 - P = 0.1 MPa

Temperature (K)
Distance from the bottom burner (cm)
ϕ_{CH} =0.70 - P = 0.3 MPa

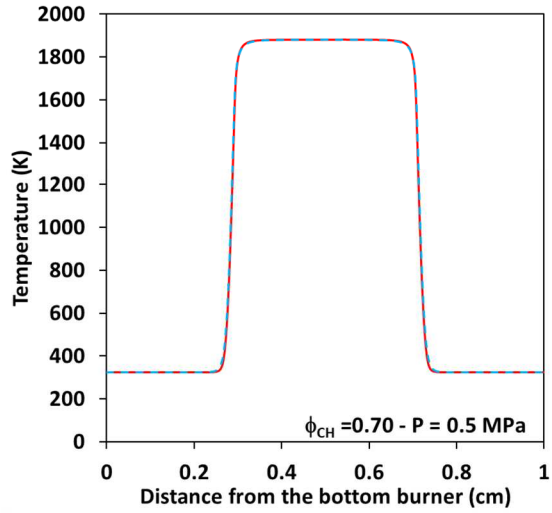
Temperature (K)
Distance from the bottom burner (cm)
ϕ_{CH} =0.70 - P = 0.5 MPa

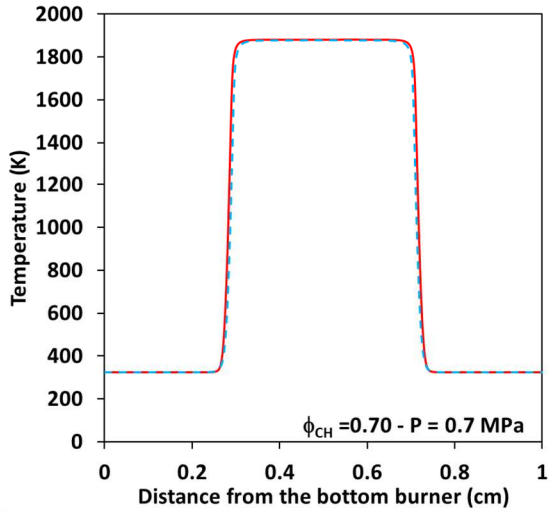
Temperature (K)
Distance from the bottom burner (cm)
ϕ_{CH} =0.70 - P = 0.7 MPa

c)

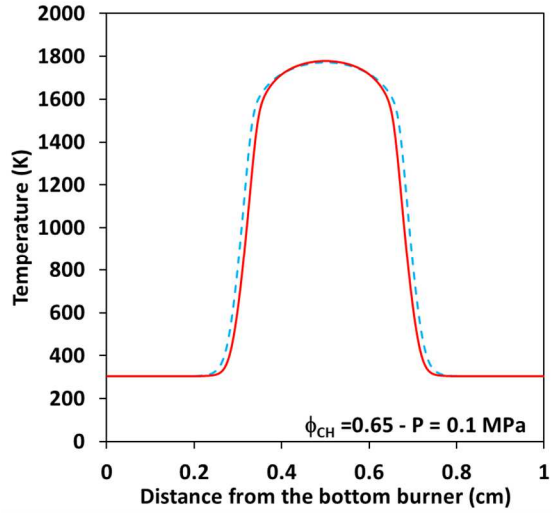
Temperature (K)
Distance from the bottom burner (cm)
ϕ_{CH} =0.65 - P = 0.1 MPa

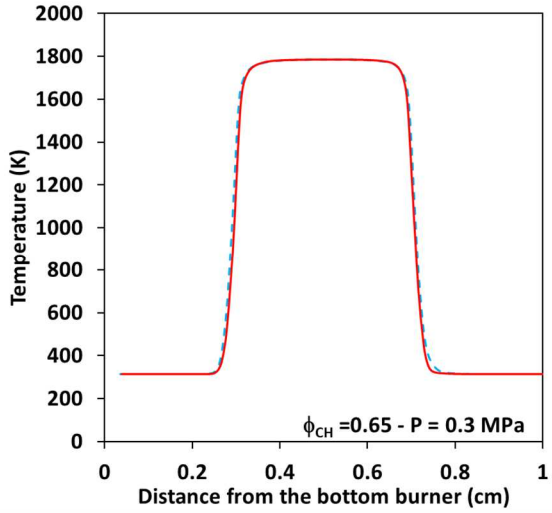
Temperature (K)
Distance from the bottom burner (cm)
ϕ_{CH} =0.65 - P = 0.3 MPa

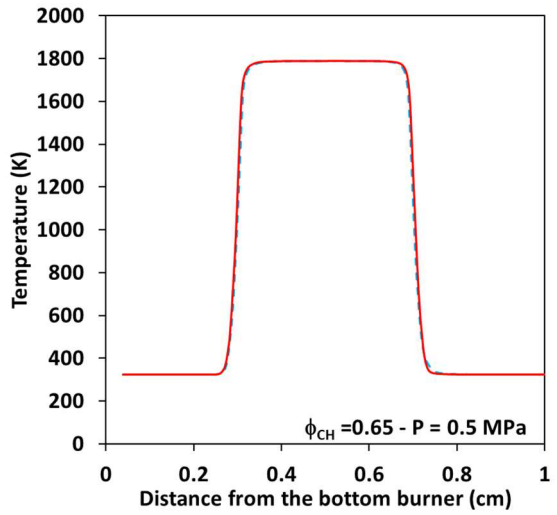
2000
1800
1600
1400
1200
1000
800
600
400
200
0
Temperature (K)
0
0.2
0.4
0.6
0.8
1
Distance from the bottom burner (cm)
ϕCH =0.65 - P = 0.5 MPa

d)

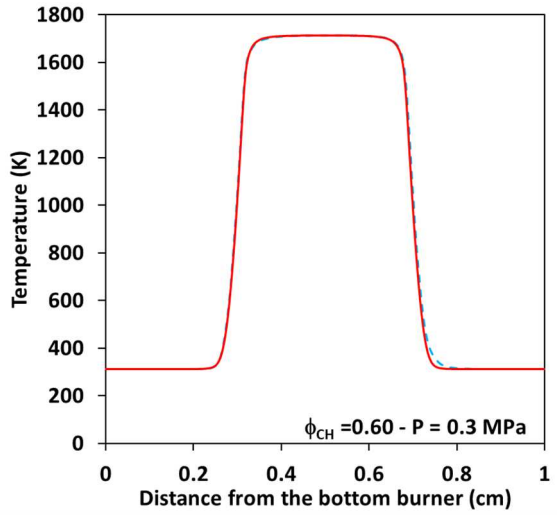
1800
1600
1400
1200
1000
800
600
400
200
0
Temperature (K)
0
0.2
0.4
0.6
0.8
1
Distance from the bottom burner (cm)
ϕCH =0.60 - P = 0.3 MPa

Table A

Normalized sensitivity coefficients of NO to reaction rate coefficients: a) ϕ_C=0.7 (ϕ_{CH}=0.74) at pressures from 0.1 to 0.7 MPa; b) ϕ_C=0.66 (ϕ_{CH}=0.7) at pressures from 0.1 to 0.7 MPa; c) ϕ_C=0.61 (ϕ_{CH}=0.65) at pressures ranging from 0.1 to 0.5 MPa; d) ϕ_C=0.57 (ϕ_{CH}=0.6) at 0.3 MPa for GDFkin®3.0_NOmecha2.0 (in red, left column) and Klippenstein mechanism (in blue, right column).

ϕ_{CH}=0.74	GDFkin30_NOmecha2.0				Klippenstein mechanism			
Reaction	0.1 MPa	0.3MPa	0.5MPa	0.7MPa	0.1 MPa	0.3MPa	0.5MPa	0.7MPa
Common reactions to both mechanisms								
$H+O_2 \rightarrow O+OH$	1	1	1	1	1	1	1	1
$O+OH \rightarrow H+O_2$	-0.6	-0.29	-0.24	-0.22	-0.7	-0.25	-0.21	-0.18
$N_2O+H \rightarrow N_2+OH$	-0.46	-0.11	0	0	-0.42	-0.1	0	0
$CH_3+O \rightarrow CH_2O+H$	-0.35	-0.12	-0.06	0	-0.16	0	0	0
$H_2O+O \rightarrow 2OH$	-0.35	-0.18	0.13	0.13	-0.46	-0.26	-0.18	-0.16
$2OH \rightarrow H_2O+O$	0.36	0.17	0.11	0.1	0.46	0.24	0.16	0.14
$H+O_2+M \rightarrow HO_2+M$	-0.27	-0.39	-0.45	-0.49	-0.27	-0.36	-0.41	-0.45
$CO+OH \rightarrow CO_2+H$	0.51	0.38	0.34	0.32	0.52	0.39	0.34	0.31
$CO_2+H \rightarrow CO+OH$	-0.16	-0.08	-0.06	-0.06	-0.19	-0.1	-0.08	-0.07
$NNH \rightarrow N_2+H$	-0.13	0	0	0	-0.19	0	0	0
$N_2+H \rightarrow NNH$	0.14	0	0	0	0.19	0	0	0
$CH_3+H+M \rightarrow CH_4+M$	0.17	-0.2	-0.2	-0.2	-0.21	-0.25	-0.25	-0.24
$H_2+OH \rightarrow H_2O+H$	0.22	0.19	0.17	0.17	0.24	0.2	0.19	0.18
$CH+N_2 \rightarrow NCN+H$	0.39	0.14	0.08	0.06	0.24	0	0	0
$N_2O+H \rightarrow NH+NO$	0.48	0.15	0.08	0	0.38	0.11	0.05	0
$N_2+O \rightarrow N+NO$	0.59	0.16	0.1	0.08	0.75	0.23	0.13	0.11
$N_2+O+M \rightarrow N_2O+M$	0.64	0.22	0.12	0.09	0.58	0.2	0.1	0.07
Different reactions between the two mechanisms								
$HCO+M \rightarrow H+CO+M$	-0.2	0.19	0.17	0.15	_	_	_	_
$CH_3+OH \rightarrow CH_2+H_2O$	0.19	0.1	0.08	0.07	_	_	_	_
$CH_2+OH \rightarrow CH+H_2O$	0.25	0.11	0.07	0	_	_	_	_
$CH+O_2 \rightarrow HCO+O$	_	_	_	_	-0.21	0	0	0
$N_2O+O \rightarrow 2NO$	_	_	_	_	0.16	0.08	0	0
$CH_2+H \rightarrow CH+H_2$	_	_	_	_	0.23	0.07	0	0

ϕ_{CH}=0.70	GDFkin30_NOmecha2.0				Klippenstein mechanism			
Reaction	0.1 MPa	0.3MPa	0.5MPa	0.7MPa	0.1 MPa	0.3MPa	0.5MPa	0.7MPa
Common reactions to both mechanisms								
$H+O_2 \rightarrow O+OH$	1	1	1	1	1	1	1	1
$O+OH \rightarrow H+O_2$	-0.59	-0.28	-0.24	-0.21	-0.7	-0.26	-0.21	-0.18
$N_2O+H \rightarrow N_2+OH$	-0.53	-0.11	0	0	-0.49	-0.1	0	0
$CH_3+O \rightarrow CH_2O+H$	-0.35	-0.1	0	0	-0.16	0	0	0
$H_2O+O \rightarrow 2OH$	-0.4	-0.14	0.13	0.13	-0.5	-0.22	-0.18	-0.12

$2OH \rightarrow H_2O+O$	0.41	0.14	0.08	-0.08	0.49	0.21	0.16	0.1
$H+O_2+M \rightarrow HO_2+M$	-0.32	-0.44	-0.51	-0.55	-0.32	-0.41	-0.41	-0.51
$CO+OH \rightarrow CO_2+H$	0.51	0.38	0.34	0.32	0.52	0.38	0.34	0.31
$N_2+H \rightarrow NNH$	0.14	0	0	0	0.2	0	0	0
$CH_3+H+M \rightarrow CH_4+M$	0.16	-0.19	-0.19	-0.19	-0.21	-0.24	-0.25	-0.22
$H_2+OH \rightarrow H_2O+H$	0.21	0.18	0.17	0.16	0.23	0.2	0.19	0.18
$CH+N_2 \rightarrow NCN+H$	0.39	0.12	0.07	0.05	0.23	0	0	0
$N_2O+H \rightarrow NH+NO$	0.55	0.14	0.07	0.05	0.43	0.11	0.05	0
$N_2+O \rightarrow N+NO$	0.48	0.1	0.06	0.05	0.6	0.15	0.13	0.07
$N_2+O+M \rightarrow N_2O+M$	0.76	0.22	0.12	0.09	0.69	0.21	0.1	0.08
$HCO+M \rightarrow H+CO+M$	-0.2	0.2	0.18	0.16	0.17	0.2	0.19	0.2
Different reactions between the two mechanisms								
$CO_2+H \rightarrow CO+OH$	-0.13	0	0	0	_	_	_	_
$N_2O+O \rightarrow 2NO$	0.14	0	0	0	_	_	_	_
$CH_2+OH \rightarrow CH+H_2O$	0.25	0.1	0.06	0	_	_	_	_
$CH_3+OH \rightarrow CH_2+H_2O$	0.2	0.09	0.07	0.07	_	_	_	_
$CH+O_2 \rightarrow HCO+O$	_	_	_	_	-0.21	0	0	0
$CH_2+H \rightarrow CH+H_2$	_	_	_	_	0.23	0	0	0
$NNH \rightarrow N_2+H$	_	_	_	_	-0.19	0	0	0

ϕ_{CH}=0.65	GDFkin30_NOmecha2.0			Klippenstein mechanism		
Reaction	**0.1 MPa**	**0.3MPa**	**0.5MPa**	**0.1 MPa**	**0.3MPa**	**0.5MPa**
Common reactions to both mechanisms						
$H+O_2 \rightarrow O+OH$	1	1	1	1	1	1
$O+OH \rightarrow H+O_2$	-0.62	-0.28	-0.23	-0.73	-0.26	-0.21
$N_2O+H \rightarrow N_2+OH$	-0.64	-0.11	-0.05	-0.59	-0.11	0
$H_2O+O \rightarrow 2OH$	-0.46	-0.13	0.12	-0.54	-0.2	-0.13
$2OH \rightarrow H_2O+O$	0.46	0.12	-0.07	0.52	0.18	0.11
$H+O_2+M \rightarrow HO_2+M$	-0.43	-0.53	-0.6	-0.42	-0.5	-0.56
$CO+OH \rightarrow CO_2+H$	0.5	0.37	0.33	0.5	0.37	0.32
$N_2+H \rightarrow NNH$	0.15	0	0	0.2	0	0
$NNH \rightarrow N_2+H$	-0.14	0	0	0.2	0	0
$CH_3+H+M \rightarrow CH_4+M$	0.15	-0.18	-0.17	-0.22	-0.22	-0.21
$H_2+OH \rightarrow H_2O+H$	0.19	0.17	0.16	0.22	0.19	0.17
$N_2O+O \rightarrow 2NO$	0.21	0.07	0	0.31	0.11	0.07
$CH+N_2 \rightarrow NCN+H$	0.39	0.1	0.05	0.22	0	0
$N_2O+H \rightarrow NH+NO$	0.64	0.13	0.07	0.48	0.11	0.06
$N_2+O \rightarrow N+NO$	0.32	0	0	0.39	0.08	0
$N_2+O+M \rightarrow N_2O+M$	0.94	0.22	0.12	0.85	0.23	0.13
$HCO+M \rightarrow H+CO+M$	0.24	0.23	0.19	0.2	0.22	0.22
Different reactions between the two mechanisms						
$CH_3+O \rightarrow CH_2O+H$	-0.34	-0.07	0	_	_	_
$CH_3+OH \rightarrow CH_2+H_2O$	0.21	0.08	0.07	_	_	_
$CH_2+OH \rightarrow CH+H_2O$	0.26	0.08	0	_	_	_

$CH+O_2 \rightarrow HCO+O$	_	_	_	-0.21	0	0
$CH_2+H \rightarrow CH+H_2$	_	_	_	0.23	0	0
$NNH+O \rightarrow NH+NO$	_	_	_	0.14	0	0

ϕ_{CH}=0.60	GDFkin30_NOmecha2.0	Klippenstein clean CF2018
Reaction	**0.3 MPa**	**0.3 MPa**
Common reactions to both mechanisms		
$H+O_2 \rightarrow O+OH$	1	1
$O+OH \rightarrow H+O_2$	-0.27	-0.27
$N_2O+H \rightarrow N_2+OH$	-0.11	-0.12
$H_2O+O \rightarrow {}_2OH$	-0.13	-0.2
$2OH \rightarrow H_2O+O$	0.12	0.18
$H+O_2+M \rightarrow HO_2+M$	-0.61	-0.58
$HCO+O_2 \rightarrow CO+HO_2$	-0.16	-0.2
$HO_2+OH \rightarrow H_2O+O_2$	-0.12	-0.08
$CO+OH \rightarrow CO_2+H$	0.35	0.35
$CH_3+H+M \rightarrow CH_4+M$	-0.17	-0.2
$H_2+OH \rightarrow H_2O+H$	0.16	0.18
$H_2O+H \rightarrow H_2+OH$	-0.08	-0.09
$N_2O+O \rightarrow 2NO$	0.08	0.14
$N_2O+H \rightarrow NH+NO$	0.13	0.11
$N_2+O+M \rightarrow N_2O+M$	0.23	0.26
$HCO+M \rightarrow H+CO+M$	0.24	0.24
Different reactions between the two mechanisms		
$CH_3+OH \rightarrow CH_2+H_2O$	0.07	_
$CH_2+OH \rightarrow CH+H_2O$	0.07	_
$H+HO_2 \rightarrow 2OH$	0.07	_
$CH+N_2 \rightarrow NCN+H$	0.12	_
$CH_2O+OH \rightarrow HCO+H_2O$	_	-0.08
$N_2O+M \rightarrow N_2+O+M$	_	-0.07
$CH_3+OH \rightarrow CH_2(S)+H_2O$	_	0.08
$CH_3+HO_2 \rightarrow CH_3O+OH$	_	0.14